Research article

Journal of RAMAN SPECTROSCOPY

Received: 20 August 2012 Revised: 28 October 2012 Accepted: 5 November 2012 Published online in Wiley Online Library: 25 January 2013

(wileyonlinelibrary.com) DOI 10.1002/jrs.4233

CW measurements of resonance Raman profiles, line-widths, and cross-sections of fluorescent dyes: application to Nile Blue A in water and ethanol

Antoine Reigue,[a,b] Baptiste Auguié,[a] Pablo G. Etchegoin[a]* and Eric C. Le Ru[a]*

The aim of this work is to illustrate the power of recently developed methods for measuring resonance Raman scattering (RRS) spectra of efficient fluorophores (using a standard continuous wave excitation and a charge-coupled device (CCD)-based Raman spectrometer), by applying them to a detailed study of a specific fluorophore: Nile Blue A. A combination of methods are used to measure the RRS properties of Nile Blue A in water (quantum yield (QY) of 4%) and ethanol (QY of 22%) at excitation wavelengths between 514 and 647 nm, thus covering both pre-resonance and RRS conditions. Standard Raman measurements are used in situations where the fluorescence background is small enough to clearly observe the Raman peaks, while the recently introduced polarization-difference RRS and continuously shifted Raman scattering are used closer to (or at) resonance. We show that these relatively straightforward methods allow us to determine the Raman cross-sections of the most intense Raman peaks and provide an accurate measurement of their line-width; even for broadenings as low as ~ 4 cm $^{-1}$. Moreover, the obtained Raman excitation profiles agree well with those derived from the optical absorption by a simple optical transform model. This study demonstrates the possibility of routine RRS measurements using standard Raman spectrometers, as opposed to more complicated time-resolved techniques. Copyright © 2013 John Wiley & Sons, Ltd.

Supporting information may be found in the online version of this article.

Keywords: resonance Raman; fluorescence rejection; Raman cross-section; Raman excitation profile; Nile Blue

Introduction

Routine measurement of resonance Raman (RR) spectra of strongly fluorescing molecules has been a long-standing goal of Raman spectroscopy.[1–7] Since Raman cross-sections are several orders of magnitude larger at resonance than off-resonance, acquiring RR spectra is *a priori* much easier and in principle can be achieved at much smaller concentrations. In practice, however, most molecules fluoresce strongly when excited at or close to resonance. Even for fluorophores with quantum yields (QYs) as low as $\sim$ 0.1%, the fluorescence background will typically overwhelm the much weaker RR peaks and preclude their observation. This issue may also affect Raman measurements of non-resonant molecules, where extrinsic fluorescence is often present, in particular in the blue-green part of the visible spectrum. Much effort has been devoted over the years to circumvent this fundamental limitation. Up until recently, the most successful approach was based on picosecond or femtosecond time-resolved Raman spectroscopy[8–15] and utilizes the fact that Raman scattering is instantaneous, while fluorescence is delayed (with fluorescence lifetimes ranging typically in the picosecond to tens of nanoseconds range). On top of the obvious increase in experimental complexity, time-resolved methods also have limitations in terms of spectral resolution and are challenging to apply to fluorophores with more moderate QYs (and therefore shorter fluorescence lifetimes). Alternative approaches include background rejection techniques by physical means using for example polarization modulation and lock-in detection[16,17] or phase-resolved[18] measurements, but these are typically far from achieving the level of background rejection required for RR scattering (RRS).

In principle, the fluorescence background could also be removed by subtraction when post-processing the data,[19–21] making use of the fact that it is a broad smooth background, as opposed to the narrow Raman peaks. The advantage of this approach is that it is very general and can be implemented on any Raman spectrometer, including those with charge-coupled device (CCD)-based detection. Although this approach works to some extent, it quickly faces fundamental limitations. First, large signal intensities are intrinsically nosier (in absolute terms), as the statistical shot-noise scales with $\sqrt{N}$ (where N is the number of photons). This can be compensated by longer integration time to reduce the relative noise (scaling as $1/\sqrt{N}$), until it is smaller than the Raman-to-background ratio. However, even then, there is another source of noise associated with the pixel-to-pixel imperfection

* *Correspondence to: Pablo G. Etchegoin, Eric C. Le Ru, The MacDiarmid Institute for Advanced Materials and Nanotechnology, School of Chemical and Physical Sciences, Victoria University of Wellington, PO Box 600, Wellington 6140, New Zealand*
E-mails: eric.leru@vuw.ac.nz; pablo.etchegoin@vuw.ac.nz

a *The MacDiarmid Institute for Advanced Materials and Nanotechnology, School of Chemical and Physical Sciences, Victoria University of Wellington, PO Box 600, Wellington 6140, New Zealand*

b *ICFP, Département de Physique de l'ENS, 24 rue Lhomond, 75005, Paris, France*

of CCD detectors.[22] This noise has a well-defined fixed structure that scales with signal intensity and cannot therefore be removed by longer integrations (for details, see supplementary information in Ref.[6]). This noise is the dominant one in CCD-based RR measurements and typically prevents the observation of RR peaks. Two similar methods were proposed to remove this noise, by taking differences between two spectra with almost the same fluorescence background (and therefore the same fixed structure noise): shifted-excitation Raman difference spectroscopy (SERDS)[23–29] and subtracted shifted Raman spectroscopy (SSRS).[22,30,31] These methods work by shifting slightly the position of the Raman peaks on the CCD, either by changing the excitation wavelength in the case of SERDS, or by moving the monochromator grating position for SSRS. Because the fluorescence background is almost unchanged, the difference spectrum has in principle no background nor fixed structure noise and, provided the shot-noise is small enough, contains the difference of two shifted RR spectra (akin to the derivative spectrum), from which the original Raman spectrum can be inferred by post-processing. These methods have indeed been applied in isolated studies,[32–35] although they have not been shown to work on difficult cases of fluorophores with moderate-to-good QYs. The main disadvantage of these (in addition to the limited availability of suitable laser lines for SERDS) is that obtaining the RR spectrum from the difference spectrum requires post-processing, typically with assumptions about the line-shapes of the Raman spectra.[23,30,26,27]

Recently, we have proposed two new methods to further improve on this work and have shown that they were capable of measuring RR spectra in the most difficult cases (like rhodamine 6G excited at 514 nm). The first one, continuously shifted Raman spectroscopy (CSRS)[7] is similar to SSRS but is based on a large number of small grating shifts (instead of just two or three as in SSRS). The main advantage is that it then allows to directly obtain the actual Raman spectrum (rather than a derivative). However, the method is so sensitive that it also picks up other peaks in the spectra, in particular those associated with (normally extremely weak) absorption lines of oxygen and water vapour in the collection path. These interfere with Raman measurements in the red part of the spectrum. For these, one may use instead the second method, polarization-difference (PD) RRS,[6] which is based on a careful subtraction of two spectra obtained in parallel and perpendicular polarization configurations.

In this work, we demonstrate explicitly how these two new methods can be used jointly to study the RR properties of fluorophores across the visible range. To this end, we focus specifically on the dye Nile Blue A, which is commonly used for biological staining[36,37] and in various contexts in surface-enhanced Raman scattering (SERS) experiments,[5,38–44] notably in connection with electrochemistry.[45,46] One of the characteristics of this dye is that its QY strongly varies depending on the nature of the solvent[37] (in particular its polarity), which allows us to illustrate the methods for representative fluorescence QYs whilst using the same dye. In fact, it has also been reported that the QY may also depend on the counter ion,[37] which may explain differences in the reported QY (for example a QY of 1% in water is reported in Refs.[47,37]). Specifically, we focused on two solvents, water (where we measured the QY to be 4%) and ethanol (QY of 22%), for which the absorption properties are similar. We obtained RR cross-sections and the RR excitation profile (RREP) of the main Raman peak of Nile Blue A (NB) at 595 cm^{-1} (attributed to a collective 'ring-breathing mode' of the structure) for excitations at 514, 531, 568, 633, and 647 nm (therefore spanning the electronic resonance). The cross-sections and RREP of the 1647 cm^{-1} mode (previously attributed to a NH_2 deformation[47]) were also determined for NB in water. We also measured with a relatively high spectral resolution how the linewidths of the Raman peaks were affected by excitation wavelength and solvent. We show that the measured RREPs agree remarkably well with predictions of a simple optical transform model,[48,49] which only takes the optical absorption as input parameter. We believe this work demonstrates clearly the possibility of routine RR measurements of fluorescent dyes using appropriate combinations of these recently developed methods.

The paper is organized as follows: in the next section, we briefly discuss the sources of noise in continuous wave CCD-based RR measurements. Note that because of space restrictions, the experimental methods and main definitions for Raman and fluorescence cross-section are provided in Sec. S.I of the Supplementary Information. In the following section, we then discuss selected examples of measurements carried out with each of the methods used in this study. Additional graphs for all the other cases are provided as supplementary information. Finally, the results are summarized, compared to theoretical predictions, and discussed in the final section.

Sources of noise in RR measurements

The main sources of noise relevant to CCD-based RR measurements have been described in detail in Refs[6,7]. In short, in the presence of a large fluorescence background, increasing the integration times reduces the shot-noise (photon noise), but this approach quickly faces limitations because of the presence of a fixed-structure noise associated primarily with the imperfection/non-uniformity of the CCD array. As illustrated in Fig. 1(a), this fixed-structure noise is of the order of $\varepsilon_f \approx 0.17\,\%$ in our experimental conditions. For a peak with Raman-to-fluorescence ratio, R, much larger than ε_f, a direct Raman measurement is possible using standard methods, and the cross-section can be readily inferred by comparison with a reference standard. As we shall see, this is possible for NB/water at 514 and 531 nm for both main Raman peaks, and at 568 nm for the 595 cm^{-1} peak only. In fact, the Raman cross-sections for these cases have previously been measured using standard techniques.[50] Closer to resonance, however, R becomes comparable to, and even much smaller than ε_f. For NB/ethanol, even off-resonance, the residual (including extrinsic) fluorescence is sufficiently strong to make R comparable to ε_f and render a direct measurement difficult. For all these cases, we therefore use the recently developed method of CSRS,[7] which provides a versatile approach of removing the fixed-structure noise.

However, the sensitivity of the method is such that it unravels new sources of noise for the lowest Raman-to-fluorescence ratios. Notably, weak absorption by oxygen and water in the atmosphere (along the collecting optical path) results in many narrow absorption lines appearing as extremely weak dips in the fluorescence spectrum, with relative amplitude typically $10^{-4} - 10^{-3}$ of the original fluorescence signal. Since these are comparable to (possibly larger than) the Raman-to-fluorescence ratio, they prevent the observation of shot-noise-limited Raman spectra in regions where these absorption bands are present.

Using a publicly available database of high-resolution spectroscopic measurements of absorption in atmospheric gases (HITRAN2008[51]), we can in fact predict accurately the positions and relative amplitudes of these absorption lines in our system. In fact, as shown in Ref.[7], the agreement with experiments is remarkable. In Fig. 1(b), we show the results of such predictions over the range of wavelengths relevant to this study (see also Fig. S4 in

Journal of RAMAN SPECTROSCOPY

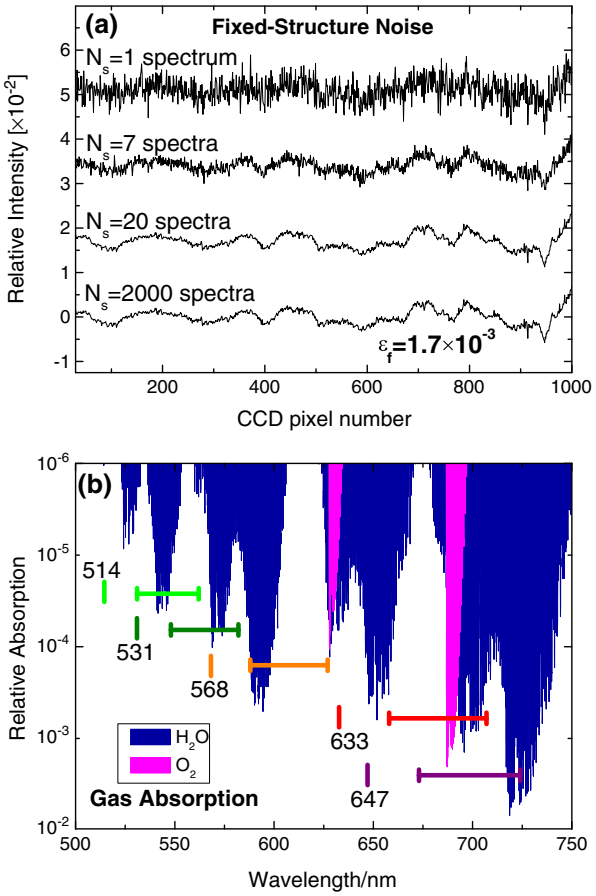

Figure 1. Sources of noise in CCD-based RR measurements. (a) Relative noise spectrum (obtained by subtracting a fourth-order polynomial from the fluorescence spectrum and normalizing by the signal of this original spectrum) for increasing number of averaged spectra (i.e. number of collected photons). The relative noise (estimated as the standard deviation of the relative background-subtracted spectrum) decreases up to a limit $\varepsilon_f = 0.17\%$ characterizing the fixed structure noise of the CCD. By comparison, the shot-noise-limited relative noise for $N_s = 2000$ (equivalent to 3×10^8 photons per CCD column) should be of the order of $\varepsilon = 6 \times 10^{-5}$. (b) Predicted relative absorption (R_A) from oxygen (pink, 20.8% concentration in air at 20 °C) and water (blue, assuming 65% humidity at 20 °C) along a path length of 6.5 m (corresponding to our experiment). The spectra are computed using the HITRAN database,[51] assuming a Gaussian instrumental broadening of 0.65 cm^{-1} (FWHM). For clarity, we use an appropriate log-scale by plotting $[-log_{10}(R_A)]$ and arbitrarily setting $R_A = 10^{-6}$ for all $R_A < 10^{-6}$ (to avoid the logarithm divergence). The laser and Raman peak positions are also indicated as in Figure 2.

the Supporting Information for an expanded version). It is clear that water absorption lines can be particularly problematic in the region 717–732 nm, with relative absorption R_A of the order of $10^{-3} - 10^{-2}$, and similarly for oxygen and water in the region 687–707 nm, with R_A of the order of $10^{-4} - 10^{-3}$. These will affect RR measurements at 633 nm for Raman peaks in the range 1200–2200 cm^{-1} and at 647 nm for Raman peaks in the range 900–1800 cm^{-1}. There are also weaker absorption lines between 568 and 633 nm at a level above $R_A \approx 10^{-4}$, which may also affect the most sensitive RR measurements in this region.

There are in principle at least three ways of overcoming the problem of gas absorption bands: One may try to remove them by post-processing the data. Indeed, using the predictions based on the HITRAN database, it is possible to predict them quite accurately. However, subtracting them exactly from the CSRS spectrum remains a challenge as it is very sensitive to small imperfections in the wavelength calibration and modelling realistically the instrumental broadening is difficult. In our experience, the magnitude of the strongest absorption lines can be reduced by a factor of 5–10 at best by post-processing, but improving this factor further is very challenging. An example of this approach is given in Fig. S20 (Supporting Information) for the 595 cm^{-1} mode of NB in ethanol at 633 nm. Another alternative is to physically remove or reduce the cause of these absorption lines by either reducing the collection pathlength or simply removing the gases responsible (for example by pumping nitrogen inside the spectrometer, or reducing as much as possible the moisture content of the ambient atmosphere). Although this would solve the problem, it is obviously not straightforward to implement. The third alternative is to use another recently proposed method for RR Spectroscopy: PD-RRS.[6] This method consists in taking the difference between two spectra obtained for parallel and perpendicular polarization configuration. Because the Raman depolarization ratio is smaller (it is often 1/3 at resonance) than the fluorescence depolarization ratio (close to 1), part of the Raman peak remains in the difference spectrum, while the fluorescence background, and its associated fixed-structure and absorption lines can be cancelled exactly with appropriate care. The disadvantage of this method compared to CSRS is that the remaining Raman peak in the difference is about twice as small, and an assumption about the Raman depolarization ratio is necessary to extract the cross-section (typically $\rho^R = 1/3$ can be assumed in resonance from theoretical arguments).

Experimental results

In this section, we will describe representative experimental results for each of the three methods that we have used in this study: direct measurement when the Raman-to-fluorescence ratio is large enough, CSRS otherwise, and PD-RRS when CSRS is hindered by gas absorption lines. The complete set of results will then be summarized and discussed in the next section. We summarize in Table 1 the methods used for each case along with the measured value of the Raman-to-fluorescence ratio for parallel polarization, $R^{\parallel}$, in each case. Note that the value of $R^{\parallel}$ off-resonance is affected by extrinsic fluorescence (especially in ethanol) and should therefore be viewed as indicative only as it may depend on the specific sample under study. In all cases where it was possible, we have tried to measure the RR spectra and cross-section for both parallel and perpendicular polarizations (the latter being much more challenging since it is typically three times weaker). This allowed us to derive the Raman depolarization ratio, ρ^R.

Absorption and fluorescence

The absorption and fluorescence spectra for Nile Blue in water and ethanol are shown in Fig. 2. The laser lines used for Raman excitation are also indicated, along with the position of the two main Raman peaks of NB at 595 and 1647 cm^{-1} (Raman shift). The absorbance spectrum is slightly modified in ethanol by solvation effects; its maximum position is in particular blue-shifted to 628 nm (down from 634 nm in water). This solvent dependence of Nile Blue has been previously studied.[37] The maximum of fluorescence is also slightly blue-shifted from 675 nm in water to 662 nm in ethanol. The main difference between the two solvents relates to the fluorescence efficiency, with a

Table 1. Summary of Raman-to-fluorescence ratios, $R^{\parallel}$, for parallel polarization configurations, as determined in this work for each of the cases investigated, along with the method used for the measurement (in brackets): DR for direct Raman measurement, CS for CSRS, and PD for PD-RRS. The magnitude of $R^{\parallel}$ provides a good indication of how difficult the RR measurement is. The Raman-to-fluorescence ratio, $R^{\perp}$, for the perpendicular polarization is of the order of 2.3 – 2.8 times smaller than $R^{\parallel}$

λ_L [nm]	NB/Water 595 cm^{-1}	NB/Water 1647 cm^{-1}	NB/Ethanol 593 cm^{-1}	NB/Ethanol 1645 cm^{-1}
514.5[a]	0.3 (DR)	0.16 (DR)	1.9×10^{-2} (CS)	1.3×10^{-3} (CS)
530.9[a]	1.0 (DR)	0.25 (DR)	-	-
568.2[a]	0.23 (DR)	4.9×10^{-3} (CS)	3.2×10^{-3} (CS)	4.3×10^{-4} (CS)
632.8	1.1×10^{-3} (CS)	$\leq 1.0 \times 10^{-4}$ (PD)	3.1×10^{-4} (CS)	-
647.1	7.2×10^{-4} (CS)	1.2×10^{-4} (PD)	3.8×10^{-4} (CS)	-

[a]Values of $R^{\parallel}$ for these excitation wavelengths are affected by extrinsic fluorescence and are therefore indicative of this measurement only; they are not intrinsic to NB solutions.

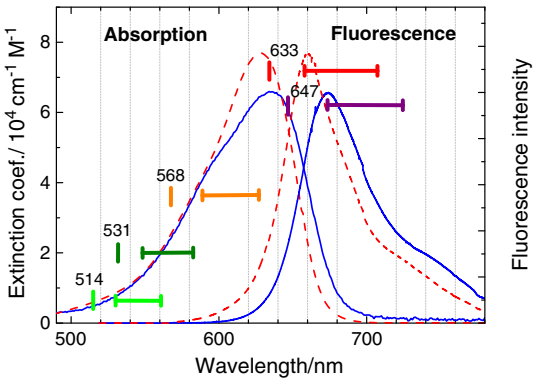

Figure 2. UV–vis absorption and fluorescence spectra (excited at 568 nm) of NB in water (blue solid lines) and ethanol (red dashed lines). The fluorescence intensities were normalized for visualization and do not reflect the actual quantum yields: 4% in water and 22% in ethanol. The vertical marks indicate the position of the laser lines used in this study, along with (to their right) the position of the two Raman peaks of NB at 595 cm^{-1} and 1647 cm^{-1}.

measured QY of the order of 4% and 22% in water and ethanol, respectively (see Fig. S3 (Supporting Information)). From the point of view of measuring RR spectra, NB/water is therefore representative of fluorophores with moderate QY, while NB/ethanol approaches the most challenging cases of good QY. For a given system, the largest fluorescence background is expected when laser excitation is at the maximum of the molecular absorption, and the Stokes–shifted Raman wavelength is close to the maximum of fluorescence emission. From Fig. 2, we see that these correspond to the 595 cm^{-1} Raman mode excited at either 647 nm for NB/water, or 633 nm for NB/ethanol. The fluorescence cross-sections in these cases is estimated to be $d\sigma^{F-}_{\Omega\bar{\nu}}(595\ cm^{-1}) = 2.4 \times 10^{-22}$ $cm^2/sr/cm^{-1}$ for NB/water at 647 nm and $d\sigma^{F-}_{g\bar{a}\bar{\nu}}(595\ cm^{-1}) = 1.7 \times 10^{-21}$ $cm^2/sr/cm^{-1}$ for NB/ethanol at 633 nm. As we shall see, measuring the 1647 cm^{-1} mode is as challenging as the 595 cm^{-1} one, because it is both weaker and broader thus resulting in a smaller Raman-to-fluorescence ratio.

Direct Raman measurements

Standard Raman measurements have been used for a number of off-resonance cases as given in Table 1. We illustrate it in Fig. 3 for NB/Water/595 cm^{-1} at 568 nm, for both polarizations. From the fit in Fig. 3(b) and a comparison to the Raman spectrum of 2-Bromo-2-Methylpropane (2B2MP) under identical conditions, we can deduce the Raman cross-section, which for parallel configuration is $d\sigma^{R-}_{\Omega} = 1.9 \times 10^{-25} cm^2/sr$. A fit of the peak in the perpendicular configuration (see Fig. S9, Supporting Information) also allows us to determine the depolarization ratio $\rho^R = I^{\perp}/I^{\parallel} = 0.35$.

CSRS

As soon as the laser excitation gets closer to the resonance (in fact even in many pre-resonance cases), the large fluorescence

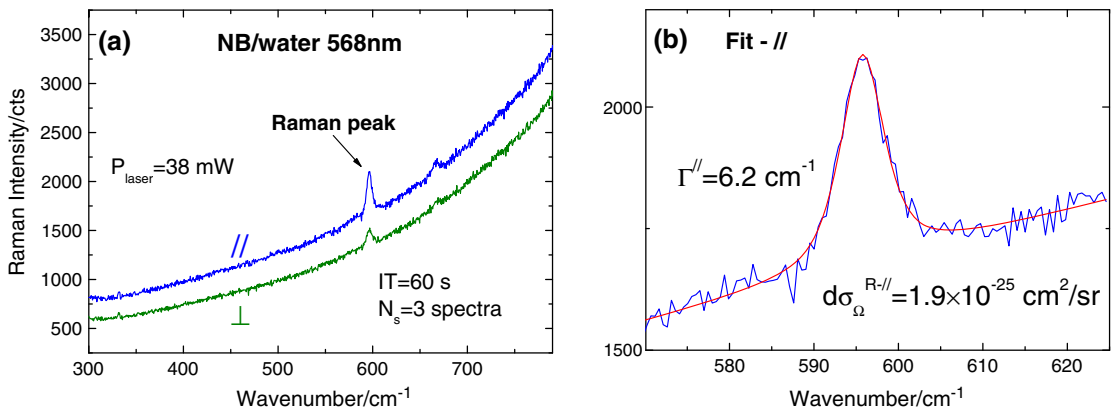

Figure 3. (a) Spectra of NB in water ($c = 0.9\ \mu$ M) for parallel and perpendicular polarizations. The fluorescence is weak, and we can see the Raman peak for both polarizations. The absolute cross-sections are inferred by comparison with a Raman spectrum of 2-Bromo-2-Methylpropane (2B2MP) taken under the same experimental conditions. (b) Raman peak region (parallel polarization only) and fit from which the line-width $\Gamma^{\parallel}$ (FWHM) and Raman cross-section $d\sigma^{R-}_{\Omega}$ are deduced. Another fit of the peak for the perpendicular polarization (see Figure S9) is carried out to deduce the Raman depolarization ratio $\rho^R = 0.35$.

Journal of RAMAN SPECTROSCOPY

background prevents the observation of the Raman peak. For NB/ethanol, this is in fact the case at all excitation wavelengths under investigation, partly because of extrinsic fluorescence. Even after subtraction of the smooth fluorescence background (typically using a fourth-order polynomial fit), the residual fixed-structure noise (with relative amplitude of the order of 0.2% of the original signal, see Fig. 1(a)) affects the quality of the measurement and can even in some cases be much larger than the Raman peaks. In such cases, the recently introduced CSRS method[7] provides a relatively easy and versatile method to remove the fixed-structure noise and recover the Raman spectrum. This method is illustrated in Fig. 4 for the 595 cm^{-1} mode of NB/ethanol at 647 nm (i.e. close to the absorption resonance and fluorescence maximum).

The fluorescence spectrum around the region of the Raman peak is shown in Fig. 4(a). It can be used to quantify the fluorescence cross-section at the Raman peak position $d\sigma^{F}_{\Omega\bar{\nu}}$ by comparison with 2B2MP. This measurement is carried out at low laser power and low NB concentration to avoid problems associated with

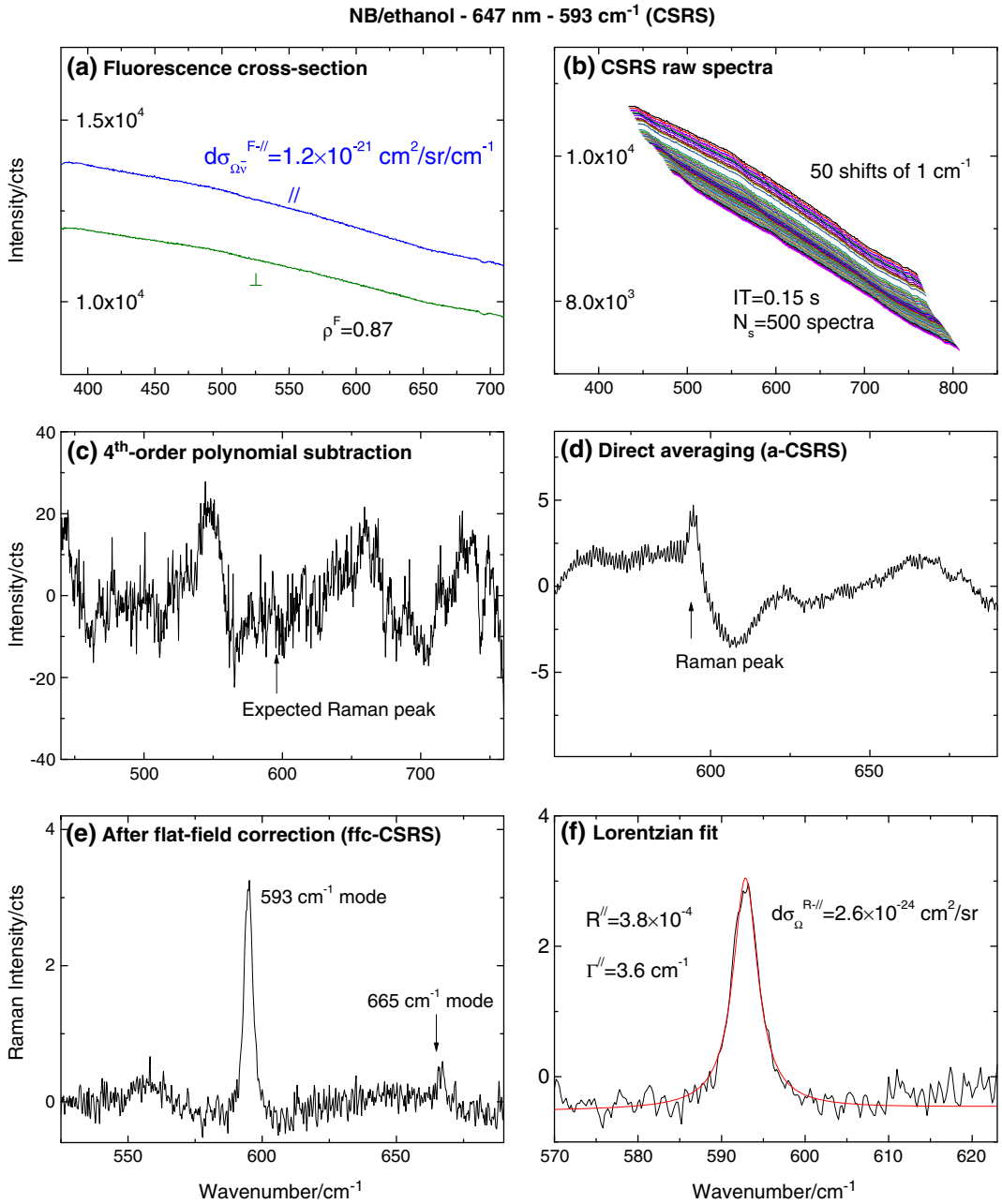

Figure 4. Illustration of a CSRS measurement for the 593 cm^{-1} mode of Nile Blue in ethanol at 647 nm excitation. (a) Fluorescence spectra of Nile Blue in ethanol for parallel and perpendicular polarizations, from which the fluorescence cross-section is deduced by comparison to 2B2MP. (b) Average spectra for each grating shift. (c) Residual after fourth-order polynomial subtraction from the fluorescence spectrum obtained at a single grating shift, showing the fixed structure noise. (d) Average of the residuals of (b) after fourth-order polynomial subtractions and shifting the spectra to equivalent grating position (a-CSRS). The fixed-structure noise is partially averaged-out in the process and the Raman peak is visible. (e) Result of the flat-field-corrected CSRS (ffc-CSRS) analysis after two iterations, (see Ref.[7] for further details) which entirely removes the fixed-structure and recovers a flat shot-noise-limited spectrum. (f) Lorentzian fit of (e) from which the properties of the Raman peak are extracted.

strong absorption of the laser and/or Raman light and with photobleaching. The Raman cross-section will then be inferred using the fluorescence background as reference, which is self-normalizing with respect to absorption and photobleaching. This two-step determination of the absolute Raman cross-section[6] allows one to ignore absorption and photobleaching issues during the CSRS measurement and therefore to maximize signal intensity.

As explained in detail in Ref.[7], the CSRS method consists in acquiring a large number of spectra (typically ~ 10 to ~ 1000 spectra) for ~ 50 small incremental shifts (typically $\sim$ 1–2 cm^{-1}) of the diffraction grating, as shown in Fig. 4(b). We average 50 spectra here over a total integration time of about 75 s for each of the 50 grating shifts. The total measurement time is therefore just over an hour, with an average of 3.6×10^9 photons collected per CCD bin (operated here in the lowest gain mode of 15 photons/cts to avoid saturation). The fixed-structure noise is evident in Fig. 4(c) from a simple background subtraction from the spectrum obtained at a single shift. As discussed in Ref.[7], the fixed-structure-free spectrum can then be recovered in two ways. The first alternative is a simple averaging of the 50 spectra after shifting them back to the same position (in practice, this requires interpolation). The obtained averaged CSRS (a-CSRS) spectrum is akin to what would be obtained from a so-called Kiefer-scan[52] and is shown in Fig. 4(d). The Raman peak is now clearly visible, but on top of a non-trivial background that would prevent any serious analysis of the line-width and line-shape. We therefore in most cases use instead the second type of analysis called flat-field corrected CSRS (ffc-CSRS) with 2 iterations (see Ref.[7] for details), which results in the almost-background-free spectrum of Fig. 4(e), also shown in Fig. 4(f) along with a Lorentzian fit to the peak. We can clearly see here that the peak is Lorentzian within experimental uncertainties. The determination of the line-width, Raman cross-section, and depolarization ratios then proceeds as described earlier for a direct Raman measurement, except that the fluorescence cross-section and fluorescence intensity under the peak are used as reference to determine the absolute Raman cross-section.

We can also deduce from this the Raman-to-fluorescence ratio, $R^{\parallel}$, which is of the order of 4×10^{-4} here, a remarkably small relative signal, which should be contrasted with the high quality of the final ffc-CSRS spectrum obtained in Fig. 4(e–f). Even the secondary Raman peak at 665 cm^{-1} is observable. This small value also explains why the peak was barely visible in the fixed-structure noise of Fig. 4(c).

PD-RRS

As discussed earlier and in Fig. 1(b), weak absorption lines of oxygen and water vapour in air may preclude the observation of the Raman peak in resonance conditions, in particular in the red part of the visible spectrum. Such a situation appears for the 1647 cm^{-1} mode excited at 647 nm. This is illustrated in Fig. 5 (a–b) where the RR spectrum obtained from the ffc-CSRS method is shown. The absorption lines with relative amplitude up to 5×10^{-3} completely hide the Raman peak with much weaker relative intensity ($R^{\parallel} = 1.2 \times 10^{-4}$ as determined *a posteriori*). Attempts at removing these absorption lines using predicted absorption spectra from the HITRAN database were not accurate enough to recover the peak.

We can therefore instead use another recently proposed method for RRS, namely PD-RRS. This method relies on the fact that the Raman signal is more polarized than the fluorescence background. The difference spectrum between two polarizations can therefore cancel out the background (including absorption lines, which have the same polarization properties as the fluorescence background) and reveal the Raman peak. More details about the implementation of this method are given in Ref.[6], and we here only illustrate the main steps and the result in Fig. 5(c-d) for the 1647 cm^{-1} mode of NB/water at 647 nm. The resulting spectrum is still very noisy because of the extremely weak Raman-to-fluorescence ratio in this case, but is nevertheless sufficient to obtain an estimate (at least an upper bound) for the Raman cross-section.

Sources of errors and uncertainties

In many of the examples presented so far and in the additional cases given in the Supplementary Information, the spectral resolution and signal-to-noise ratio are good enough to characterize the line-shape of the peak, which can be fitted by a Lorentzian peak within experimental uncertainties in the majority of cases. In some cases, a Lorentzian fit does not appear to be adequate and a pseudo-Voigt fit is used instead. Such instances typically also exhibit a slightly larger line-width than average (compared to the same mode at other excitation wavelength), and we therefore believe that the non-Lorentzian line-shape is a consequence of non-ideal alignment conditions resulting in instrumental broadening. In fact, from multiple independent repeats of these experiments, it appears that the main source of error in the line-width estimate Γ is the instrumental broadening, which depends on the exact optical alignment and varies in the range $0.5 - 1$ cm^{-1}. The typical error on the line-width is therefore estimated to be ± 0.5 cm^{-1}. For noisier measurements of the 595 cm^{-1}, this typically increases to ± 1 cm^{-1}. The relative error is of the same order for the 1647 cm^{-1}, which means that the absolute errors are about twice as large since it is about twice as broad.

The spectra obtained for the perpendicular configuration are weaker and therefore usually noisier. This results in potentially large errors on the line-width $\Gamma^{\perp}$, which in turn affect the depolarization ratio ρ^R. In such cases, we have fixed $\Gamma^{\perp}$ to be equal to $\Gamma^{\parallel}$ in the fits. Even then, there is the possibility of a slight different optical alignment condition for the two polarization configurations (because the rotation of the lambda/2 waveplate may introduce a minute change in the laser beam position). Overall, there is therefore a relatively large error of between $\pm 10\%$ and $\pm 20\%$ in all our measurements of ρ^R. With this in mind, almost all our values of ρ^R are compatible, within experimental errors, with the value of 1/3 predicted for resonance and pre-resonance conditions with a single electronic state.

Overall, the uncertainty in the cross-section estimates is dominated by four sources: First, the uncertainty in the concentration of NB. To reduce this to a minimum, the actual concentration of all samples was characterized by UV/Vis absorption after all absolute cross-section measurements. The molar extinction coefficients given in Fig. 2 were used as a reference, and these may have an error of about 10 % associated with weighing and preparation of the original bulk solutions. This error is however the same for all our measurements. Second, the uncertainty in the line-shape of the spectrum. For example, a Gaussian fit to the Raman peak results in an integrated intensity 1.5 times smaller than a Lorentzian fit of same FWHM. This can be an issue for noisy spectra where the actual line-shape cannot be easily identified. However, we found that in most cases where the signal-to-noise ratio was good enough to study the line-shape, the Raman peaks under

Journal of RAMAN SPECTROSCOPY

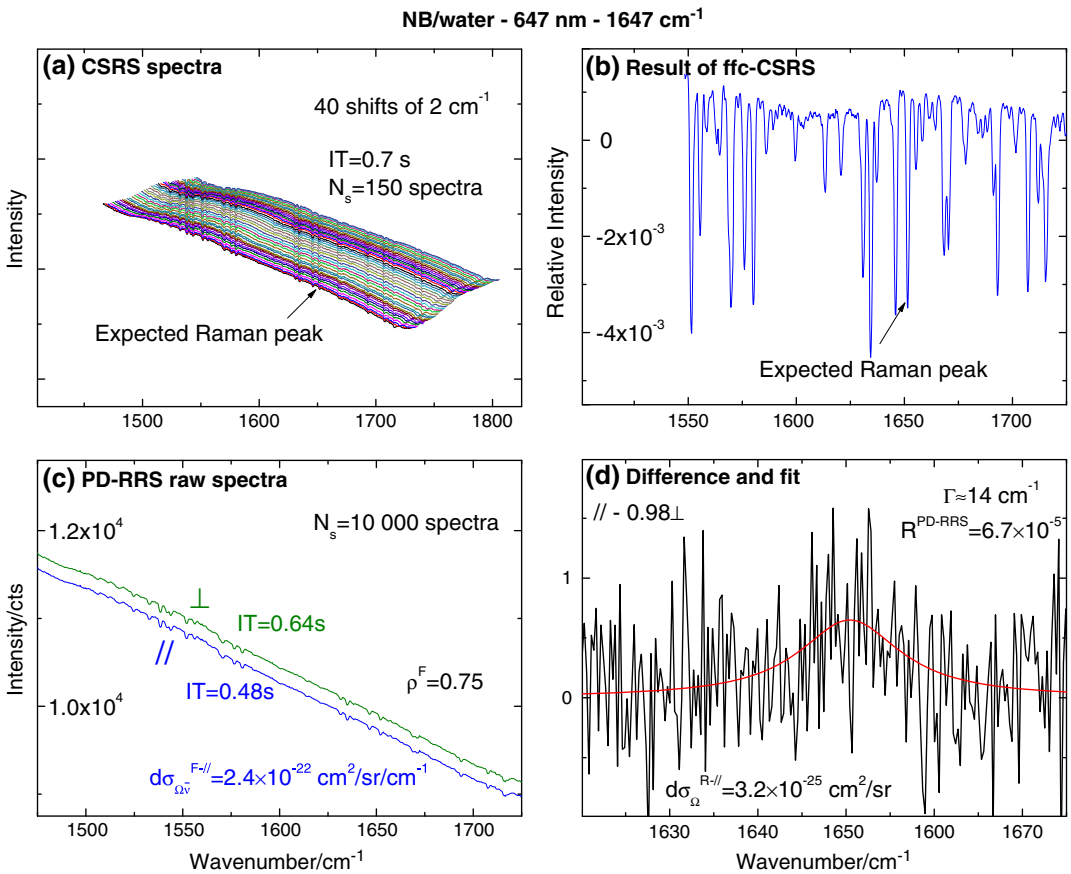

Figure 5. Example of CSRS failure and use of a PD-RRS measurement instead for the 1647 cm^{-1} mode of Nile Blue in water at 647 nm excitation. (a) CSRS average spectra for parallel polarization for each grating shifts (40 shifts of 2 cm^{-1}). (b) Result of the ffc-CSRS method showing clear water absorption bands with up to 5×10^{-3} relative intensity and preventing any observation of the Raman peak. (c) Fluorescence spectra obtained for each polarization for the PD-RRS measurement. Note the different integration times to account for the non-unity fluorescence depolarization ratio. (d) PD-RRS spectrum obtained by subtraction of the parallel and perpendicular polarizations, along with a tentative Lorentzian fit to the peak. The fixed-structure noise and water absorption bands cancel out in this subtraction. The PD-RRS cross-section ($d\sigma_{\Omega}^{PDRRS} = 1.8 \times 10^{-25}$ cm^2/sr) is inferred as for CSRS with respect to the fluorescence background intensity (from an independent measurement of the fluorescence cross-section). Assuming the Raman depolarization ratio is $\rho^R = 1/3$, the Raman cross-section is then deduced from[6] $d\sigma_{\Omega}^{R-} = d\sigma_{\Omega}^{PDRRS}\left(1 - \rho^R/\rho^F\right)^{-1}$.

study here were best described by a Lorentzian (as opposed to a Gaussian or a pseudo-Voigt) profile. Lorentzian fits were therefore used by default when the signal-to-noise ratio was not good enough to properly assess the line-shape. Third, the uncertainty in the line-width of the peak can have an important effect on the estimated integrated area (and therefore cross-section), in fact much more than the peak intensity, which is typically much more constrained during the fit. The error in Γ was discussed earlier, and this will result in a typical uncertainty of $\pm 20\,\%$ in the estimated cross-sections. This is we believe the dominant source of error in our measurement (in addition to the systematic error associated with the concentration estimate of the stock solution). The three items discussed so far affect the determination of $d\sigma_{\Omega}^{R-}$ for parallel polarization. The Raman cross-section $d\sigma_{\Omega}^{R}$ is then obtained from $d\sigma_{\Omega}^{R} = \left(1 + \rho^R\right) d\sigma_{\Omega}^{R-}$ and is therefore in addition affected by uncertainties in ρ^R discussed earlier.

To this general discussion, one should finally add the potential additional statistical errors in cases where the signal-to-noise ratio is poor. The spectra and fits used for all our measurements are provided in the Supplementary Information and provide a 'visual' guide for the errors associated with each.

Discussion

Figures with the experimental spectra, fits, and extracted values for all the cases investigated in this work are provided in the Supplementary Information for reference (S5 to S21). These graphs are useful to gauge from the noise level the errors in the parameters obtained from the fits. We summarize in Table 2 the results for the most relevant parameters.

As for the electronic properties (e.g. absorption), small differences are observed between the Raman spectra of NB in water and ethanol. The peak positions are slightly shifted, for example from 595.5 cm^{-1} and 1647 cm^{-1} in water to 593.2 cm^{-1} and 1645 cm^{-1} in ethanol. The Raman peak line-widths also appear to be narrower in ethanol than in water, at all excitation wavelengths. Such solvation effects are in fact not unexpected, but have never been explicitly resolved before in direct measurements of resonant Raman spectra with the type of resolution we have here.

Regarding the Raman cross-sections, we first note that the values obtained here off-resonance (514 and 531 nm) are comparable to those measured before for NB in ethylene-glycol.[50] The most interesting aspect of our work relates to the previously not

Table 2. Summary of the results

λ_L [nm]	514.5	530.9	568.2	632.8	647.1
NB/Wat 595 cm^{-1}					
$d\sigma_\Omega^{R-}$ [10^{-26} cm^2/sr]	3.6	5.9	19	170	160
$\Gamma^{\parallel}$ [cm^{-1}]	6.5	5.7	6.2	6.3	5.9
ρ^R	0.36	0.36	0.35	0.34	0.31
$d\sigma_\Omega^{R}$ [10^{-26} cm^2/sr]	4.9	8.0	26	230	210
NB/Wat 1647 cm^{-1}					
$d\sigma_\Omega^{R-}$ [10^{-26} cm^2/sr]	10	11	39	≤40[a]	32[a]
$\Gamma^{\parallel}$ [cm^{-1}]	15	13.3	13.6	14[a]	14[a]
ρ^R	0.39	0.40	0.35	1/3[a]	1/3[b]
$d\sigma_\Omega^{R}$ [10^{-26} cm^2/sr]	14	15.5	53	≤53[a]	43[a]
NB/Wat					
$r_{1647/595}$	2.9	1.9	2.0	≤0.23[a]	0.20[a]
NB/Eth 593 cm^{-1}					
$d\sigma_\Omega^{R-}$ [10^{-26} cm^2/sr]	3.8	-	27	380	260
$\Gamma^{\parallel}$ [cm^{-1}]	4.4	-	5.1	4.7	3.6
ρ^R	0.36	-	0.33	0.35	0.3
$d\sigma_\Omega^{R}$ [10^{-26} cm^2/sr]	5.2	-	36	510	350
NB/Eth 1645 cm^{-1}					
$d\sigma_\Omega^{R-}$ [10^{-26} cm^2/sr]	12	-	82	-	-
$\Gamma^{\parallel}$ [cm^{-1}]	11.1	-	14.2	-	-
ρ^R	0.32	-	0.34	-	-
$d\sigma_\Omega^{R}$ [10^{-26} cm^2/sr]	16	-	110	-	-

[a]These values are subject to particularly large uncertainties because of a poor signal-to-noise ratios, see figures in the suppl. info for details.
[b]$\rho^R = 1/3$ is here assumed, not measured.

measured cross-sections approaching or even at resonance (568, 633, and 647 nm) and to the corresponding Raman excitation profile (REP). As expected, there is a large increase in the Raman cross-sections at or close to resonance. However, there is also a dramatic change of relative intensities between the two Raman modes under study, the ratio $r = d\sigma_\Omega^R(1647\text{cm}^{-1})/d\sigma_\Omega^R(595\text{cm}^{-1})$ being about ten times smaller at 633 and 647 nm than at shorter wavelengths. This suggests that these two modes have a markedly different REP. The experimental results also suggest a slightly different REP for the 595 cm^{-1} mode in water and ethanol, which is a natural consequence of the slight difference in electronic properties.

In order to be more quantitative, we have used a simple optical transform model[48,49] to predict these REPs. The main advantage of this model is that it only requires a knowledge of the optical absorption but should nevertheless provide accurate predictions of REPs under a set of reasonable assumptions:[48,49] adiabatic, Condon, and harmonic approximations; single electronic state; linear electron–phonon coupling. Explicitly, following Refs.[48,49], we compute from the absorption cross-section $\sigma_{Abs}(\lambda)$ the following complex function of absolute wavenumber $\bar{\nu} = 1/\lambda$ (note the link with Kramers–Kronig relations):

$$\varphi(\bar{\nu}) = \mathcal{P}\int_0^\infty \frac{\sigma_{abs}(\bar{\nu}')}{\bar{\nu}'(\bar{\nu}'-\bar{\nu})}d\bar{\nu}' - i\pi\frac{\sigma_{abs}(\bar{\nu})}{\bar{\nu}}, \qquad (1)$$

where $\mathcal{P}$ denotes the principal value of the integral. $\varphi(\bar{\nu})$ is computed numerically from the measured $\sigma_{Abs}(\lambda)$, limiting the range of integration from 400 to 800 nm (extending the integral below 400 nm has a negligible effect on the results). The REP, $d\sigma_\Omega^R(\bar{\nu}_L)$ for a given mode with vibrational energy $\bar{\nu}_v$ excited at a wavelength $\lambda_L = 1/\bar{\nu}_L$ is then obtained from:

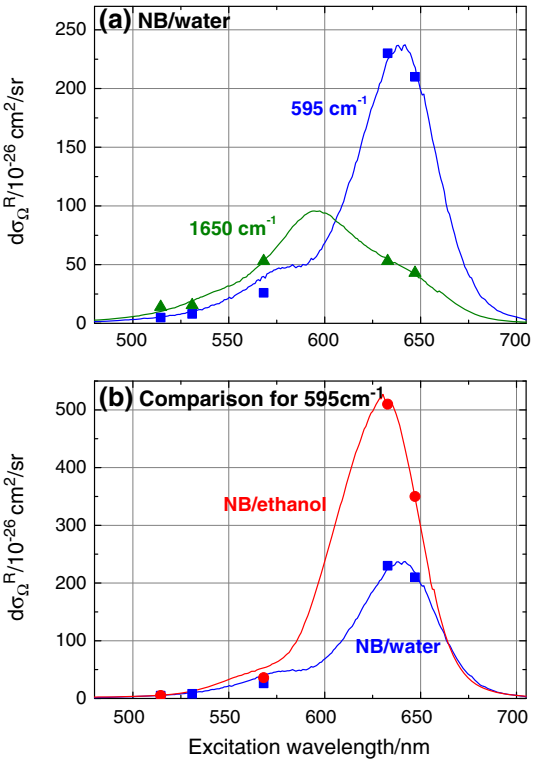

Figure 6. Raman excitation profiles computed from the optical transform model as in Eqn (2) (solid lines) along with the Raman cross-sections measured in this work (symbols). In (a), we compare the REPs of the two main modes of NB in water, while in (b), we compare the REPs of the same 595 cm^{-1} mode of Nile Blue in water and in ethanol. Note that the scaling factor for a given REP is not obtained from the model but adjusted for the best fit.

$$d\sigma_\Omega^R(\bar{\nu}_L) = A_v(\bar{\nu}_L - \bar{\nu}_v)^4\left|\varphi(\bar{\nu}_L) - \varphi(\bar{\nu}_L - \bar{\nu}_v)\right|^2, \qquad (2)$$

where A_v is a scaling factor independent of $\bar{\nu}_L$ and relates to the Franck-Condon overlap of the vibration.

The computed REPs for all cases of interest are shown in Fig. 6. These predictions agree remarkably well with the experimental results. From these, we can see that the 1647 cm^{-1} mode resonance is blueshifted down to 590 nm and its Raman intensity is substantially decreased at 633 and 647 nm, which explains the observed decrease in the ratio *r*. Other features of the experimental data are also captured by the simple theoretical model, notably the difference in Raman cross-sections of the 595 cm^{-1} at 633 and 647 nm. While they are comparable for NB in water, the small shift in electronic resonance in ethanol results in a sharp decrease in cross-section from 633 to 647 nm.

Finally, the scaling factor A_v can be derived (up to a constant factor) from the comparison with the experimental cross-sections. The theory predicts that A_v is proportional to $\Delta_v^2/\bar{\nu}_v$, where Δ_v characterizes the shift in the equilibrium position of the normal coordinates between the ground and excited electronic states.[49] Our results suggest that Δ_v is larger by a factor ≈1.5 for the 595 cm^{-1} mode compared to the 1647 cm^{-1} mode.

Conclusions

In closing, we believe we have provided a full worked-out example of the application of new techniques to study resonant Raman

spectra with conventional Raman systems, in situations that have been considered very difficult or impossible in the past (because of the interference with fluorescence). REPs for the example treated here agree well with predictions from an optical transform model that only requires the absorption as an input, and reference cross-sections for NB can now be used in other branches of Raman spectroscopy where they are relevant (for example, in single-molecule SERS). We believe the examples chosen here illustrate the power of the techniques and anticipate that similar studies can be readily extended to other fluorescent dyes of interest.

Acknowledgements

ECLR is indebted to the Royal Society of New Zealand (RSNZ) for support through a Marsden Grant and Rutherford Discovery Fellowship. PGE acknowledges support from a Marsden Grant of the RSNZ.

Supporting information

Supporting information may be found in the online version of this article.

References

[1] D. A. Long, *The Raman effect, a unified treatment of the theory of Raman scattering by molecules*, John Wiley & Sons Ltd., Chichester, **2002**.
[2] R. L. McCreery, *Raman Spectroscopy for Chemical Analysis*, John Wiley & Sons, Inc., **2005**.
[3] E. V. Efremov, F. Ariese, C. Gooijer, *Anal. Chim. Acta* **2008**, *606*, 119.
[4] A. Myers Kelley, *J. Phys. Chem. A* **2008**, *112*, 11975.
[5] E. C. Le Ru, P. G. Etchegoin, *Principles of Surface Enhanced Raman Spectroscopy and Related Plasmonic Effects*, Elsevier, Amsterdam, **2009**.
[6] E. C. Le Ru, L. C. Schroeter, P. G. Etchegoin, *Anal. Chem.* **2012**, *84*, 5074.
[7] B. Auguié, A. Reigue, E. C. Le Ru, P. G. Etchegoin, *Anal. Chem.* **2012**, *84*, 7938.
[8] P. Matousek, M. Towrie, A. W. Parker, J. Raman *Spectrosc.* **2002**, *33*, 238.
[9] W. M. Kwok, C. Ma, P. Matousek, A. W. Parker, D. Phillips, W. T. Toner, M. Towrie, S. Umapathy, *J. Phys. Chem. A* **2001**, *105*, 984.
[10] A. C. Benniston, P. Matousek, I. E. McCulloch, A. W. Parker, M. Towrie, *J. Phys. Chem. A* **2003**, *107*, 4347–4353.
[11] P. Kukura, D. W. McCamant, S. Yoon, D. B. Wandschneider, R. A. Mathies, *Science* **2005**, *310*, 1006–1009.
[12] C. Fang, R. R. Frontiera, R. Tran, R. A. Mathies, *Nature* **2009**, *462*, 200.
[13] R. Wilbrandt, *Biospectroscopy* **1996**, *2*, 263.
[14] E. Efremov, J. Buijs, C. Gooijer, F. Ariese, *Appl. Spectrosc.* **2007**, *61*, 571.
[15] S. Shim, C. M. Stuart, R. A. Mathies, *Chemphyschem* **2008**, *9*, 697.
[16] C. A. Arguello, G. F. Mendes, R. C. C. Leite, *Appl. Optics* **1974**, *13*, 1731.
[17] S. M. Angel, M. K. DeArmond, K. W. Hanck, D. W. Wertz, *Anal. Chem.* **1984**, *56*, 3000.
[18] A. Z. Genack, *Anal. Chem.* **1984**, *56*, 2957.
[19] T. Hasegawa, J. Nishijo, J. Umemura, *Chem. Phys. Lett.* **2000**, *317*, 642.
[20] T. Vickers, R. Wambles Jr., C. Mann, *Appl. Spectrosc.* **2001**, *55*, 389.
[21] Z.-M. Zhang, S. Chen, Y.-Z. Liang, Z.-X. Liu, Q.-M. Zhang, L.-X. Ding, F. Ye, H. Zhou, *J. Raman Spectrosc.* **2010**, *41*, 659.
[22] S. Bell, E. Bourguignon, A. Dennis, *Analyst* **1998**, *123*, 1729.
[23] A. P. Shreve, N. J. Cherepy, R. A. Mathies, *Appl. Spectrosc.* **1992**, *46*, 707.
[24] P. A. Mosier-Boss, S. H. Lieberman, R. Newbery, *Appl. Spectrosc.* **1995**, *49*, 630.
[25] J. Zhao, M. Carrabba, F. Allen, *Appl. Spectrosc.* **2002**, *56*, 834.
[26] P. Matousek, M. Towrie, A. Parker, *Appl. Spectrosc.* **2005**, *59*, 848.
[27] I. Osticioli, A. Zoppi, E. Casteilucci, *J. Raman Spectrosc.* **2006**, *37*, 974.
[28] M. Maiwald, G. Erbert, A. Klehr, H.-D. Kronfeldt, H. Schmidt, B. Sumpf, G. Tränkle, *Appl. Phys. B* **2006**, *85*, 509.
[29] S. McCain, R. Willett, D. Brady, *Opt. Express* **2008**, *16*, 10975.
[30] A. O'Grady, A. Dennis, D. Denvir, J. McGarvey, S. Bell, *Anal. Chem.* **2001**, *73*, 2058.
[31] S. Bell, E. Bourguignon, A. O'Grady, J. Villaumie, A. Dennis, *Spectrosc. Europe* **2002**, *14*, 17.
[32] S. E. J. Bell, E. S. O. Bourguignon, A. C. Dennis, J. A. Fields, J. J. McGarvey , K. R. Seddon, *Anal. Chem.* **2000**, *72*, 234.
[33] Y. Oshima, Y. Komachi, C. Furihata, H. Tashiro, H. Sato, *Appl. Spectrosc.* **2006**, *60*, 964.
[34] I. Osticioli, A. Zoppi, E. Castellucci, *Appl. Spectrosc.* **2007**, *61*, 839.
[35] M. A. da Silva Martins, D. G. Ribeiro, E. A. P. dos Santos, A. A. a. Martin, A. Fontes, H. da Silva Martinho, *Biomed. Opt. Express* **2010**, *1*, 617.
[36] A. G. Ostle, J. G. Holt, *Appl. Environ. Microbiol.* **1982**, *44*, 238.
[37] J. Jose, K. Burgess, *Tetrahedron* **2006**, *62*, 11021.
[38] A. M. Glass, P. F. Liao, J. G. Bergman, D. H. Olson, *Opt. Lett.* **1980**, *5*, 368.
[39] U. Nickel, A. zu Castell, K. Poppl, S. Schneider, *Langmuir* **2000**, *16*, 9087.
[40] E. C. Le Ru, E. Blackie, M. Meyer, P. G. Etchegoin, *J. Phys. Chem. C* **2007**, *111*, 13794.
[41] P. G. Etchegoin, E. C. Le Ru, *Anal. Chem.* **2010**, *82*, 2888.
[42] S. A. Meyer, E. C. Le Ru, P. G. Etchegoin, *Anal. Chem.* **2011**, *83*, 2337.
[43] E. C. Le Ru, S. A. Meyer, C. Artur, P. G. Etchegoin, J. Grand, P. Lang, F. Maurel, *Chem. Comm.* **2011**, *47*, 3903.
[44] E. C. Le Ru, J. Grand, I. Sow, W. R. C. Somerville, P. G. Etchegoin, M. Treguer-Delapierre, G. Charron, N. Felidj, G. Levi, J. Aubard, *Nano Lett.* **2011**, *11*, 5013.
[45] F. Ni, H. Feng, L. Gorton, T. M. Cotton, *Langmuir* **1990**, *6*, 66–73.
[46] E. Cortes, P. G. Etchegoin, E. C. Le Ru, A. Fainstein, M. E. Vela, R. C. Salvarezza, *J. Am. Chem. Soc.* **2010**, *132*, 18034.
[47] H. Oliveira, A. Camargo, L. Macedo, M. Gehlen, A. da Silva, *Spectrochim. Acta. Part A* **2002**, *58*, 3103.
[48] D. L. Tonks, J. B. Page, *Chem. Phys. Lett.* **1979**, *66*, 449.
[49] J. B. Page, D. L. Tonks, *J. Chem. Phys.* **1981**, *75*, 5694.
[50] M. K. Lawless, R. A. Mathies, *J. Chem. Phys.* **1992**, *96*, 8037.
[51] L. Rothman, I. Gordon, A. Barbe, D. Benner, P. Bernath, M. Birk, V. Boudon, L. Brown, A. Campargue, J.-P. Champion, K. Chance, L. Coudert, V. Dana, V. Devi, S. Fally, J.-M. Flaud, R. Gamache, A. Goldman, D. Jacquemart, I. Kleiner, N. Lacome, W. Lafferty, J.-Y. Mandin, S. Massie, S. Mikhailenko, C. Miller, N. Moazzen-Ahmadi, O. Naumenko, A. Nikitin, J. Orphal, V. Perevalov, A. Perrin, A. Predoi-Cross, C. Rinsland, M. Rotger, M. Šimečková, M. Smith, K. Sung, S. Tashkun, J. Tennyson, R. Toth, A. Vandaele, J. V. Auwera, *J. Quant. Spectrosc. Rad. Transf.* **2009**, *110*, 533.
[52] V. Deckert, W. Kiefer, *Appl. Spectrosc.* **1992**, *46*, 322.

Supporting information for "CW measurements of resonance Raman profile, linewidths, and cross-sections of fluorescent dyes: application to Nile Blue A in water and ethanol"

Antoine Reigue,[1,2] Baptiste Auguié,[1] Pablo G. Etchegoin,[1*] and Eric C. Le Ru[1*]

[1] *The MacDiarmid Institute for Advanced Materials and Nanotechnology, School of Chemical and Physical Sciences, Victoria University of Wellington, PO Box 600, Wellington 6140, New Zealand.*
[2] *ICFP, Département de Physique de l'ENS , 24 rue Lhomond, 75005 Paris France.*
[*] *E-mail: eric.leru@vuw.ac.nz (ECLR), pablo.etchegoin@vuw.ac.nz (PGE)*

S.I. EXPERIMENTAL METHODS AND PRELIMINARIES

A. Definitions

We adopt here the same definitions and conventions for the various cross-sections as used in Ref. [1], which we recall here briefly for completeness. Raman cross-sections are characterized by the 90°-scattering differential Raman cross-section (spectrally integrated over the Raman peak and all outgoing polarizations), denoted by $d\sigma^R_\Omega \equiv d\sigma^R/d\Omega = d\sigma^{R-\parallel}_\Omega + d\sigma^{R-\perp}_\Omega$, typically expressed in units of [cm^2/sr]. In this expression, $d\sigma^{R-\parallel}_\Omega$ and $d\sigma^{R-\perp}_\Omega$ are the standard differential cross-sections for parallel and perpendicular polarization scattering configurations, respectively. We note that the total (integrated over solid angle) Raman cross-section σ^R [cm^2] is also sometimes used instead, [2, 3] and can be easily deduced from: [2, 4]

$$\sigma^R = \frac{8\pi}{3}\frac{1+2\rho^R}{1+\rho^R} d\sigma^R_\Omega, \tag{S1}$$

where ρ^R is the *Raman depolarization ratio*, given as:

$$\rho^R = \frac{d\sigma^{R-\perp}_\Omega}{d\sigma^{R-\parallel}_\Omega}. \tag{S2}$$

For fluorescent molecules, we are also interested in quantifying the fluorescence intensity under the Raman peak (as opposed to the total fluorescence intensity), and we will therefore use the 90°-scattering doubly-differential (with respect to solid angle Ω and wavenumber $\bar{\nu}$) fluorescence cross-section, denoted by $d\sigma^F_{\Omega\bar{\nu}} \equiv d^2\sigma^F/(d\Omega d\bar{\nu})$; which we will express in units of [cm^2/sr/cm^{-1} $\equiv$ cm^3/sr]. Note that it is not spectrally integrated and therefore depends on the spectral position (wavenumber or wavelength) at which it is evaluated (and also obviously on the excitation wavelength). This is necessary because the fluorescence has a very different spectral width from a typical Raman peak. Accordingly, we are only interested in quantifying the fluorescence over a much smaller spectral range than its natural emission width; hence the need for doubly-differential fluorescence cross-section. Note that the standard differential fluorescence cross-section $d\sigma^F_\Omega$ would be given by spectral integration as:

$$d\sigma^F_\Omega = \int d\sigma^F_{\Omega\bar{\nu}}(\bar{\nu}) d\bar{\nu}. \tag{S3}$$

From these basic cross-sections, one can in principle infer the ratio of Raman-to-fluorescence intensity, and therefore how difficult a RR measurements will be (or more quantitatively: which relative noise level ϵ is required for a direct RR measurement). For this, we however need to know the Raman peak intensity (rather than the integrated intensity) and this is also characterized by a doubly-differential (Raman) cross-section, [5] $d\sigma^R_{\Omega\bar{\nu}}$. The latter depends on the line-width (and to a lesser degree the line-shape) of the Raman peak. For a Lorentzian line-shape with Full Width at Half Maximum (FWHM) Γ, it is straightforward to show that the peak Raman intensity is, for example for parallel polarization:

$$d\sigma^{R-\parallel}_{\Omega\bar{\nu}} = \frac{2}{\pi\Gamma} d\sigma^{R-\parallel}_\Omega. \tag{S4}$$

We can therefore define, for a given Raman peak and excitation wavelength, the Raman-to-fluorescence intensity ratio in the parallel polarization configuration, $R^\parallel$ [adimensional] as:

$$R^\parallel = \frac{d\sigma^{R-\parallel}_{\Omega\bar{\nu}}}{d\sigma^{F-\parallel}_{\Omega\bar{\nu}}}, \tag{S5}$$

which provides a measure of how difficult it is to directly measure the Raman signal on top of the fluorescence background (the lower $R^\parallel$, the harder it is). We note that since $R^\parallel$ is related to the Raman peak intensity (rather than its spectrally integrated intensity), it may depend slightly on the instrumental broadening. In practice, $R^\parallel$ is simply the Raman peak intensity divided by the intensity of the background underneath it.

B. Experimental set-up

A typical experimental set-up for these experiments, based on the standard 90°-scattering configuration, is presented in Fig. S1. The detection is always performed in the (fixed) vertical direction to avoid differences in instrumental efficiencies. The excitation is either $\parallel$ or $\perp$ to

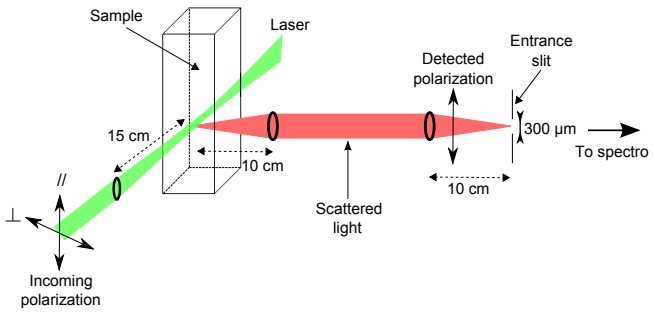

FIG. S1: Schematic of the standard 90°-scattering configuration used in these experiments.

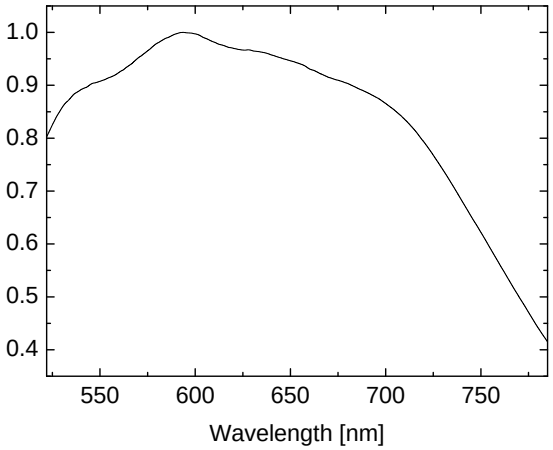

FIG. S2: System response (normalized and smoothed), calibrated using a tungsten lamp.

the detection direction (selected by an achromatic $\lambda/2$ waveplate), and is focused in the center of the cell by a $f = 15\,\mathrm{cm}$ focal length lens. The collection of the signal is performed with two lenses of focal length $f = 10\,\mathrm{cm}$ each, thus achieving an image with a magnification of one on the entrance slit of the monochromator. These experiments were performed on a T64000 Jobin-Yvon triple additive/subtractive spectrometer (used in subtractive mode) coupled to a liquid-nitrogen-cooled Symphony CCD with fast acquisition mode. The depolarization ratio (for either Raman or fluorescence) is defined as the ratio of intensities: $\rho = I_\perp/I_\parallel$.

Most of the experiments were carried out using 1800 lines/mm gratings with $200 - 300\,\mu\mathrm{m}$ entrance slit, resulting in a spectral resolution of $\approx 0.5 - 1\,\mathrm{cm}^{-1}$. For excitation, we have used either a HeNe laser (30mW at 633 nm) or an Ar/Kr laser for the other lines at 514.5, 530.9, 568.2, and 647.1 nm with typical powers up to 100 mW. In simple cases, absolute Raman and fluorescence cross-sections were characterized by comparison with the $516\,\mathrm{cm}^{-1}$ Raman peak of 2-Bromo-2-methylpropane (2B2MP) as a reference standard. [6] Its Raman cross-section at 633 nm excitation is $5.4 \times 10^{-30}\,\mathrm{cm}^2/\mathrm{sr}$ (with a depolarization of $\rho^R = 0.16$), from which the cross-section for parallel polarization at other visible wavelengths (which are still far from the resonance in the UV) is deduced as:

$$d\sigma_\Omega^{R-\parallel}(\lambda_L) = \left(\frac{10^7/(\lambda_L[\mathrm{nm}]) - 516\,\mathrm{cm}^{-1}}{15282\,\mathrm{cm}^{-1}}\right)^4 \times 4.6 \times 10^{-30}\,\mathrm{cm}^2/\mathrm{sr}. \quad \text{(S6)}$$

The correction of the reference cross-section from its value at 633 nm in Eq. S6 accounts for the well-known ω^4-dependence of off-resonance Raman cross-sections. Note that this method of comparison with 2B2MP can only be carried out on samples of sufficiently low concentration, where absorption of both laser and Raman light is negligible (typically $3 - 5\,\mu$M at most in the resonant region of NB in our configuration, with ≈ 5 mm pathlength in solution for excitation and ≈ 2 mm for collection). The system response was calibrated (see Fig. S2) using a tungsten white light source and this was taken into account when estimating cross-sections.

C. Preparation of Nile Blue solution

Nile Blue A perchlorate (NB, dye content 95%) was purchased from Sigma-Aldrich. Extra precautions must be taken for the water solution because of the poor solubility of NB in water, and its tendency to form aggregates. In fact, inconsistent results were obtained when preparing samples from a $100\,\mu$M NB/water stock solution. A 2 L stock solution of NB in water was therefore prepared at a relatively low concentration of $12\,\mu$M and magnetically stirred for a week. Other samples were then prepared by further dilution from this reference solution. Magnetic stirring of the stock solution was also carried out before any further dilution. The absorbance then scales linearly with concentration until $\approx 6\,\mu$M, [1] which therefore corresponds to the onset of creation of dye-aggregates (probably dimers). Only solutions of NB/water at concentrations below $6\,\mu$M were therefore used in the measurements. The NB/ethanol solutions were also prepared from a 2 L stock solution at $12\,\mu$M concentration. There was no evidence of solubility or dye-aggregation issues in this case.

D. Quantum yield measurements

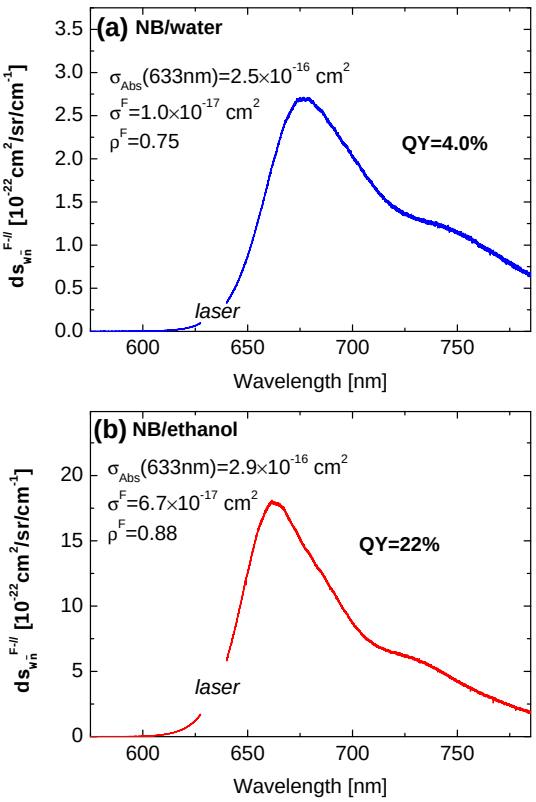

FIG. S3: Quantum yield determination for (a) $c = 0.88\,\mu$M NB/water solution and (b) $c = 0.84\,\mu$M NB/ethanol solution. Shown are the spectral dependence of the absolute doubly-differential fluorescence cross-sections for parallel polarization ($d\sigma^{F-\parallel}_{\Omega\tilde{\nu}}$), excited at 633 nm, using 2B2MP as a reference cross-section standard. The fluorescence depolarization ratio ρ^F is obtained from a similar measurement in the perpendicular polarization, and the absorption cross-section $\sigma_{\rm Abs}$ at 633 nm from UV/Vis absorption. The fluorescence differential cross-section $d\sigma^{F-\parallel}_{\Omega}$ is then obtained by spectral integration. From this, the total fluorescence cross-section is obtained as $\sigma^F = d\sigma^{F-\parallel}_{\Omega}(8\pi/3)(1+2\rho^F)/(1+\rho^F)$ and the quantum yield from $\mathrm{QY} = \sigma^F/\sigma_{\rm Abs}$.

E. Gas absorption lines

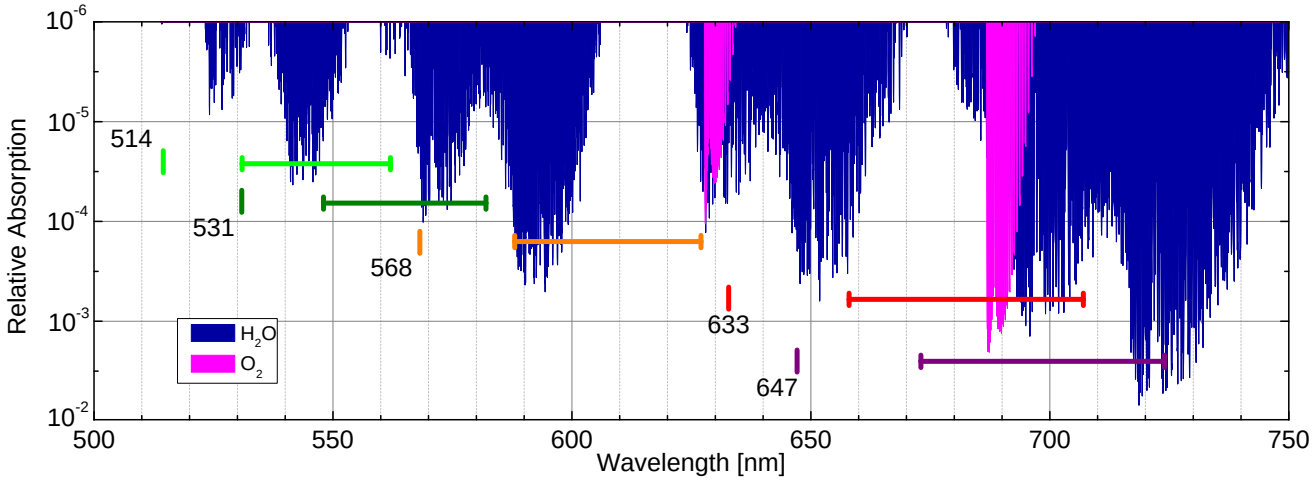

FIG. S4: This graph is simply a larger and more readable version of Fig. 2(b) of the main manuscript. It shows the predicted relative absorption (R_A) from oxygen (pink, 20.8% concentration in air at 20°C) and water (blue, assuming 65% humidity at 20°C) along a path length of 6.5 m (corresponding to our experiment). The spectra are computed using the HITRAN database, [7] assuming a Gaussian instrumental broadening of 0.65 cm^{-1} (FWHM). For clarity, we use an appropriate log-scale and plot $-\log_{10}(R_A)$ and arbitrarily set $R_A = 10^{-6}$ for all $R_A < 10^{-6}$ (to avoid the logarihtm divergence). The laser and Raman peak positions for the two peaks studied in the main paper are also indicated.

S.II. RAMAN SPECTRA AND FITS

We now provide sequentially the Raman spectra and fits obtained in each of the cases investigated. Most fits are Lorentzian with a linear background, but pseudo-Voigt fits were also used where appropriate (typically when instrumental broadening is large). The signal-to-noise ratio and quality of the fits give an indication of the reliability of the values obtained in each case. We indicate in these plots the values inferred from the fits for the differential Raman cross-section for parallel polarization $d\sigma_\Omega^{R-\parallel}$, the linewidths for both polarizations $\Gamma^\parallel$ and $\Gamma^\perp$, and the Raman depolarization ratio ρ^R. For continuously-shifted Raman spectroscopy (CSRS) [8] and polarization-difference resonance Raman spectroscopy (PD-RRS) [1] measurements, we also measure the Raman-to-fluorescence ratio $R^\parallel$, from which the Raman cross-section is deduced using the fluorescence background as a reference. In such cases, we also indicate in the caption the value of the doubly-differential fluorescence cross-section under the Raman peak, $d\sigma_{\Omega\bar{\nu}}^{F-\parallel}$, and the fluorescence depolarization ratio ρ^F, both of which are obtained from an independent measurement at low laser power. The Raman cross-section for a Lorentzian peak is then deduced from (see also Eq. 4 and 5 of the main text):

$$d\sigma_\Omega^{R-\parallel} = \frac{\pi\Gamma^\parallel}{2} R^\parallel d\sigma_{\Omega\bar{\nu}}^{F-\parallel}. \tag{S7}$$

In the case of NB in ethanol, we have when possible double-checked the results using the $884\,\mathrm{cm}^{-1}$ mode of ethanol as an alternative reference Raman cross-section standard. For this, we have measured (against 2B2MP) the differential Raman cross-section for parallel polarization at 514 nm to be $d\sigma_\Omega^{R-\parallel} = 1.1\times10^{-30}\,\mathrm{cm}^2/\mathrm{sr}$ and the Raman depolarization ratio $\rho^R = 0.18$. The cross-section for other (longer) excitation wavelengths is obtained using the ω^4-scaling factor.

Note that we have not measured NB in ethanol at 531 nm excitation and that measurements of the $1645\,\mathrm{cm}^{-1}$ mode for NB ethanol at 633 and 647 nm are not shown as they were not sensitive enough to reveal the peak (because the resonance Raman enhancement is moderate but the fluorescence background is still large).

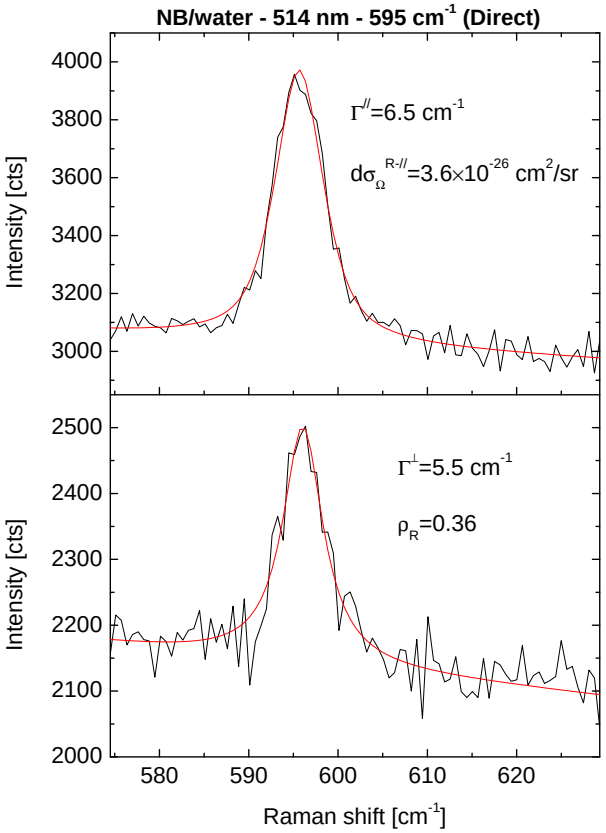

FIG. S5: Direct Raman measurement of the 595 cm^{-1} mode of NB in water ($c = 2.2\,\mu$M) at 514 nm for parallel ($\|$) and perpendicular ($\perp$) polarizations, along with pseudo-Voigt fits. Integrations times are 180 s. The cross-sections are inferred by comparison with 2B2MP. We believe the larger linewidth for $\|$ is a result of instrumental broadening due to a slight misalignment.

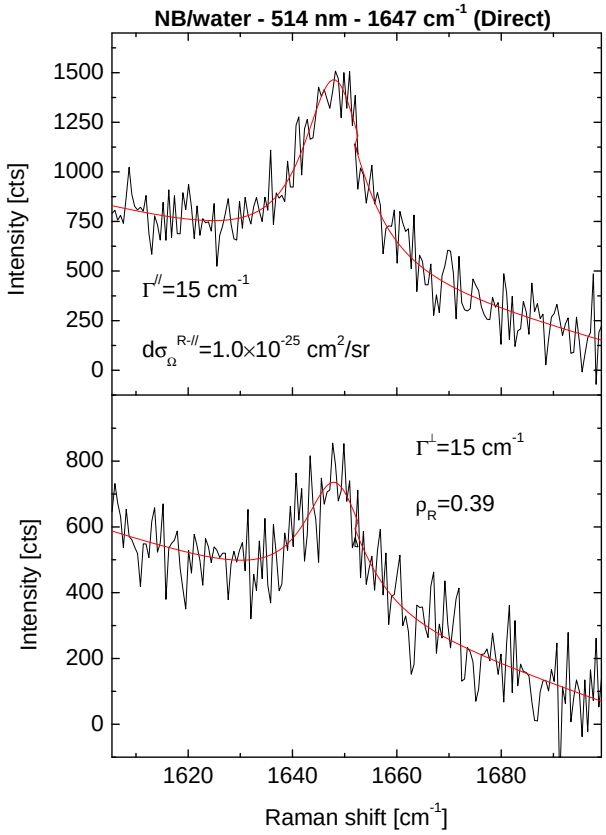

FIG. S6: Direct Raman measurement of the 1647 cm^{-1} mode of NB in water ($c = 2.2\,\mu$M) at 514 nm for parallel ($\|$) and perpendicular ($\perp$) polarizations, along with Lorentzian fits. Integrations times are 180 s. The cross-sections are inferred by comparison with 2B2MP.

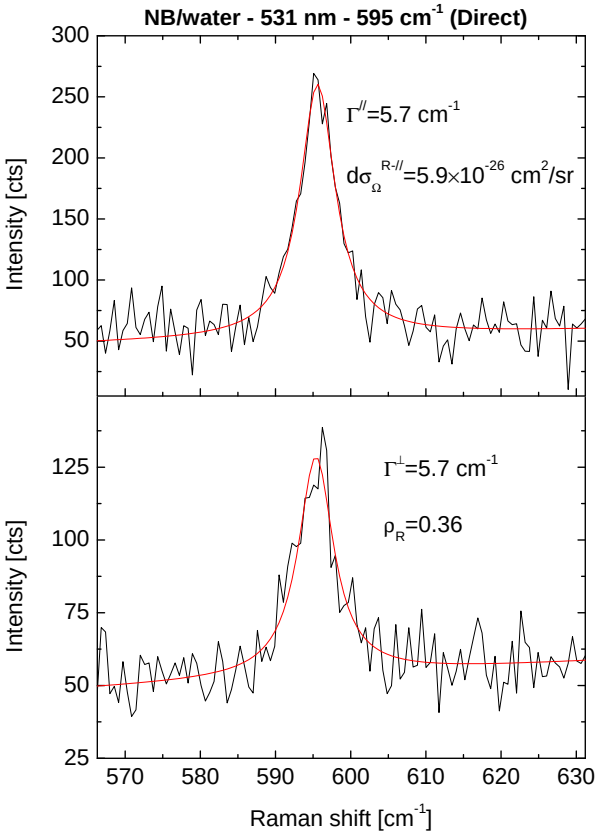

FIG. S7: Direct Raman measurement of the 595 cm^{-1} mode of NB in water ($c = 4.2\,\mu$M) at 531 nm for parallel ($\parallel$) and perpendicular ($\perp$) polarizations, along with Lorentzian fits. Integrations times are 180 s ($\parallel$) and 600 s ($\perp$). The cross-sections are inferred by comparison with 2B2MP.

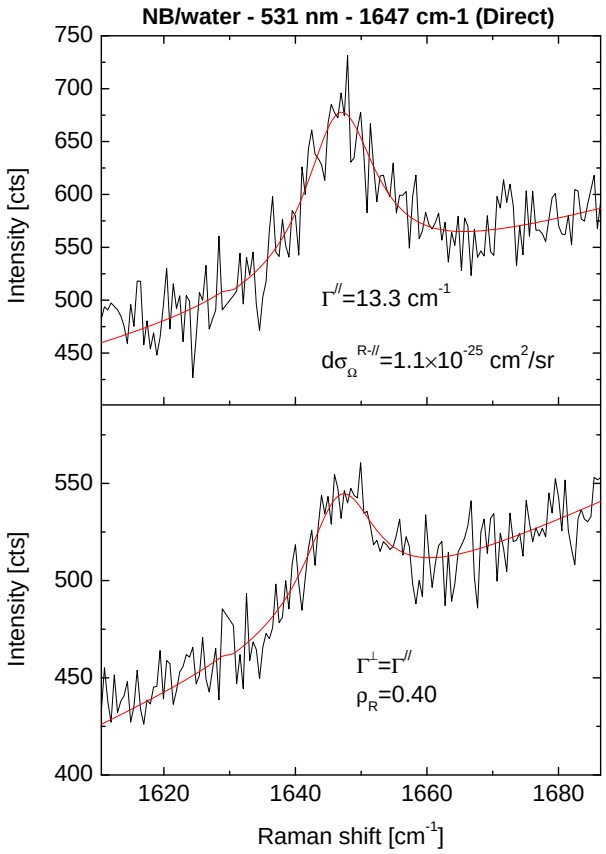

FIG. S8: Direct Raman measurement of the 1647 cm^{-1} mode of NB in water ($c = 4.2\,\mu$M) at 531 nm for parallel ($\parallel$) and perpendicular ($\perp$) polarizations, along with Lorentzian fits. We have here imposed $\Gamma^{\perp} = \Gamma^{\parallel}$ in the fit for $\perp$. Integrations times are 180 s. The cross-sections are inferred by comparison with 2B2MP.

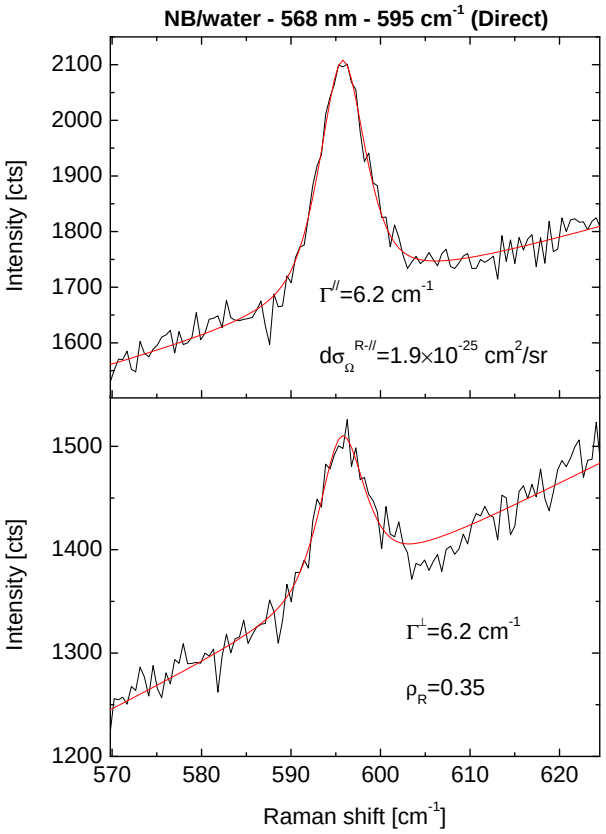

FIG. S9: Direct Raman measurement of the 595 cm^{-1} mode of NB in water ($c = 0.9\,\mu$M) at 568 nm for parallel (||) and perpendicular ($\perp$) polarizations, along with pseudo-Voigt fits (Lorentzian fits here do not seem adequate, but this is possibly related to instrumental broadening). Integrations times are 180 s. The cross-sections are inferred by comparison with 2B2MP.

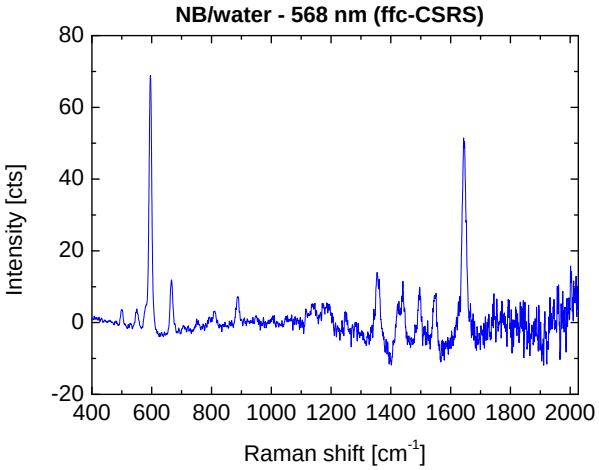

FIG. S10: CSRS measurement of the full Raman spectrum of NB in water ($c \approx 6\,\mu$M) at 568 nm, obtained using lower resolution gratings with 50 shifts of 12 cm^{-1} and 40 s integration per shift.

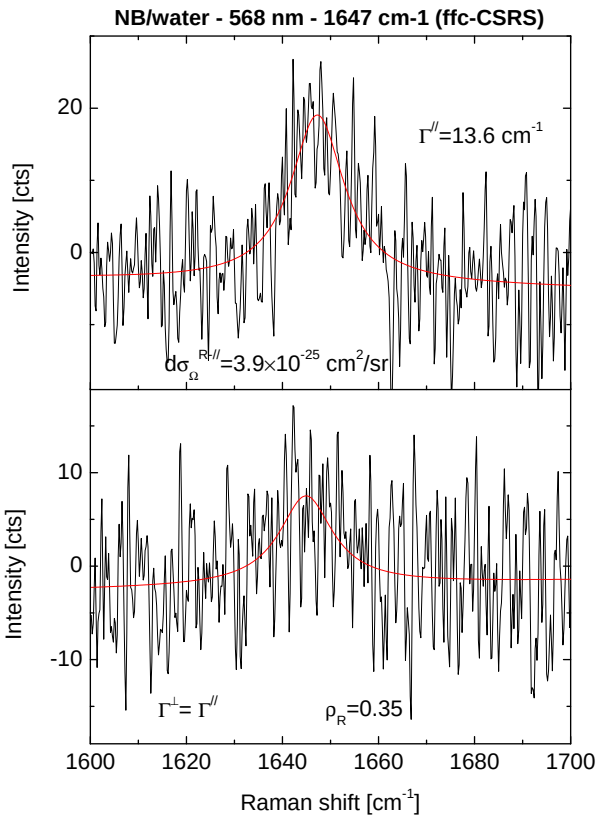

FIG. S11: CSRS measurement of the 1647 cm^{-1} mode of NB in water ($c = 4.9\,\mu$M) at 568 nm using 40 shifts of 2 cm^{-1} and 40 s integration per shift. We show the ffc-CSRS spectra for parallel (||) and perpendicular ($\perp$) polarizations, along with Lorentzian fits. We have here imposed $\Gamma^{\perp} = \Gamma^{\parallel}$ in the fit for $\perp$, but the quality of the fit remains marginal. The observed high-frequency oscillations in both cases are attributed to Fabry-Perot oscillations along the collection path (most likely inside the glass cell wall). They do not affect the fit strongly, but could nevertheless be avoided by adding a thick glass cube optically matched to the cell. [1] The cross-sections are inferred by using the fluorescence background (not shown and dominated by extrinsic fluorescence here) as a reference as explained in the main text and in Eq. S7. We here have $R^{\parallel} = 4.9 \times 10^{-3}$ and independently measured $d\sigma^{F-\parallel}_{\Omega\bar{\nu}} = 3.7 \times 10^{-24}\,\mathrm{cm}^2/\mathrm{sr}/\mathrm{cm}^{-1}$ and $\rho^F = 0.8$. Note that the same Raman cross-section is derived from a full CSRS spectrum (obtained with a lower resolution) and shown in Fig. S10, by comparing the 1647 cm^{-1} intensity to that of the 595 cm^{-1}.

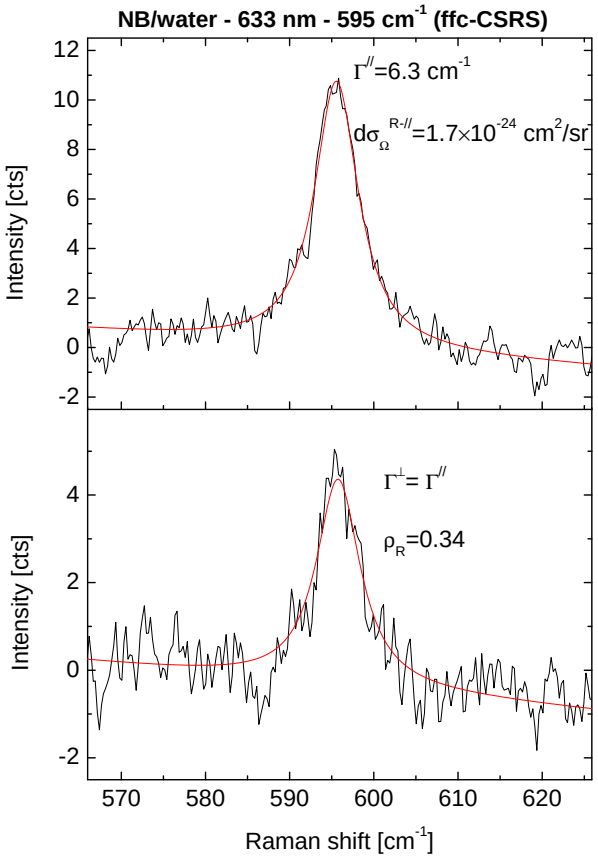

FIG. S12: CSRS measurement of the $595\,\mathrm{cm}^{-1}$ mode of NB in water ($c = 2.6\,\mu$M) at 633 nm using 50 shifts of $2\,\mathrm{cm}^{-1}$ with 56 s ($\parallel$) and 72 s ($\perp$) integration per shift. We show the ffc-CSRS (with 2 iterations) spectra for parallel ($\parallel$) and perpendicular ($\perp$) polarizations, along with Lorentzian fits. We have here imposed $\Gamma^{\perp} = \Gamma^{\parallel}$ in the fit for $\perp$. The cross-sections are inferred by using the fluorescence background (not shown) as a reference as explained in the main text and in Eq. S7. We here have $R^{\parallel} = 1.1 \times 10^{-3}$ and independently measured $d\sigma^{F-\parallel}_{\Omega\bar{\nu}} = 1.6 \times 10^{-22}\,\mathrm{cm}^2/\mathrm{sr}/\mathrm{cm}^{-1}$ and $\rho^F = 0.75$.

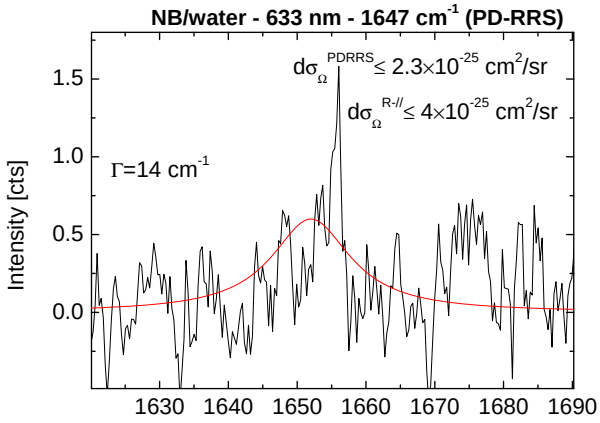

FIG. S13: PD-RRS measurement of the $1647\,\mathrm{cm}^{-1}$ mode of NB in water ($c \approx 3\,\mu$M) at 633 nm with 3400 s ($\parallel$) and 4600 s ($\perp$) integration times. We show the difference spectrum along with a tentative Lorentzian fit. Given the poor signal-to-noise ratio, we have here imposed $\Gamma = 14\,\mathrm{cm}^{-1}$ and the proposed fit should only be viewed as a way to obtain an upper estimate to the Raman cross-section rather than as a credible fit to the peak. A higher laser power (not available to us at 633 nm) would be necessary to improve this measurement. The cross-sections are inferred by using the fluorescence background (not shown) as a reference. We here have $R^{\mathrm{PDRRS}} = 5.7 \times 10^{-5}$ and independently measured $d\sigma^{F-\parallel}_{\Omega\bar{\nu}} = 1.8 \times 10^{-22}\,\mathrm{cm}^2/\mathrm{sr}/\mathrm{cm}^{-1}$ and $\rho^F = 0.75$, from which the measured PD-RRS cross-section is obtained: $d\sigma^{\mathrm{PDRRS}}_{\Omega} = 2.3 \times 10^{-25}\,\mathrm{cm}^2/\mathrm{sr}$. Assuming the Raman depolarization ratio is $\rho^R = 1/3$, the Raman cross-section is then deduced from [1] $d\sigma^{R-\parallel}_{\Omega} = d\sigma^{\mathrm{PDRRS}}_{\Omega}(1 - \rho^R/\rho^F)^{-1}$.

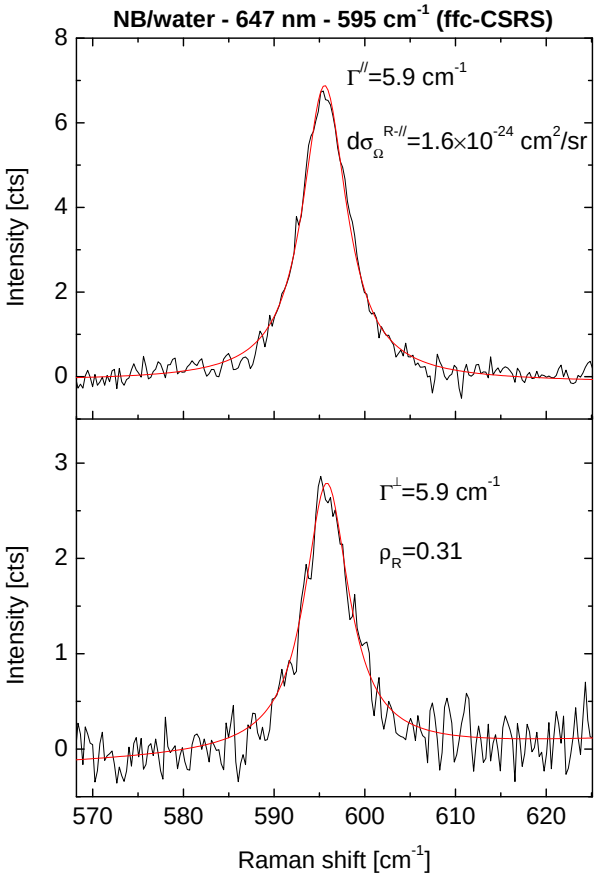

FIG. S14: CSRS measurement of the $595\,\mathrm{cm}^{-1}$ mode of NB in water ($c \approx 3\,\mu$M) at 647 nm using 50 shifts of $1\,\mathrm{cm}^{-1}$ with 60 s integration per shift. We show the ffc-CSRS (with 2 iterations) spectra for parallel ($\|$) and perpendicular ($\perp$) polarizations, along with Lorentzian fits. The cross-sections are inferred by using the fluorescence background (not shown) as a reference as explained in the main text and in Eq. S7. We here have $R^{\|} = 7.2 \times 10^{-4}$ and independently measured $d\sigma^{F-\|}_{\Omega\bar{\nu}} = 2.4 \times 10^{-22}\,\mathrm{cm}^2/\mathrm{sr}/\mathrm{cm}^{-1}$ and $\rho^F = 0.75$.

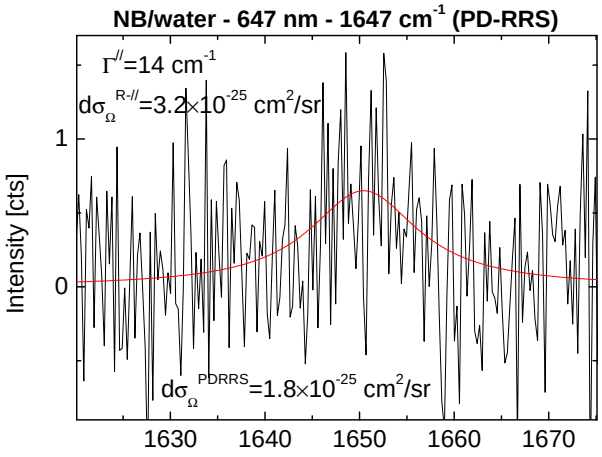

FIG. S15: PD-RRS measurement of the $1647\,\mathrm{cm}^{-1}$ mode of NB in water ($c \approx 3\,\mu$M) at 647 nm with 2900 s ($\|$) and 3900 s ($\perp$) integration times. We show the difference spectrum along with a Lorentzian fit. Given the poor signal-to-noise ratio, we have here imposed $\Gamma = 14$ in the fit, but a large uncertainty remains in the derived cross-sections. The cross-sections are inferred by using the fluorescence background (not shown) as a reference. We here have $R^{\mathrm{PDRRS}} = 6.7 \times 10^{-5}$ and independently measured $d\sigma^{F-\|}_{\Omega\bar{\nu}} = 1.2 \times 10^{-22}\,\mathrm{cm}^2/\mathrm{sr}/\mathrm{cm}^{-1}$ and $\rho^F = 0.75$, from which the measured PD-RRS cross-section is obtained: $d\sigma^{\mathrm{PDRRS}}_{\Omega} = 1.8 \times 10^{-25}\,\mathrm{cm}^2/\mathrm{sr}$. Assuming the Raman depolarization ratio is $\rho^R = 1/3$, the Raman cross-section is then deduced from [1] $d\sigma^{R-\|}_{\Omega} = d\sigma^{\mathrm{PDRRS}}_{\Omega}(1 - \rho^R/\rho^F)^{-1}$.

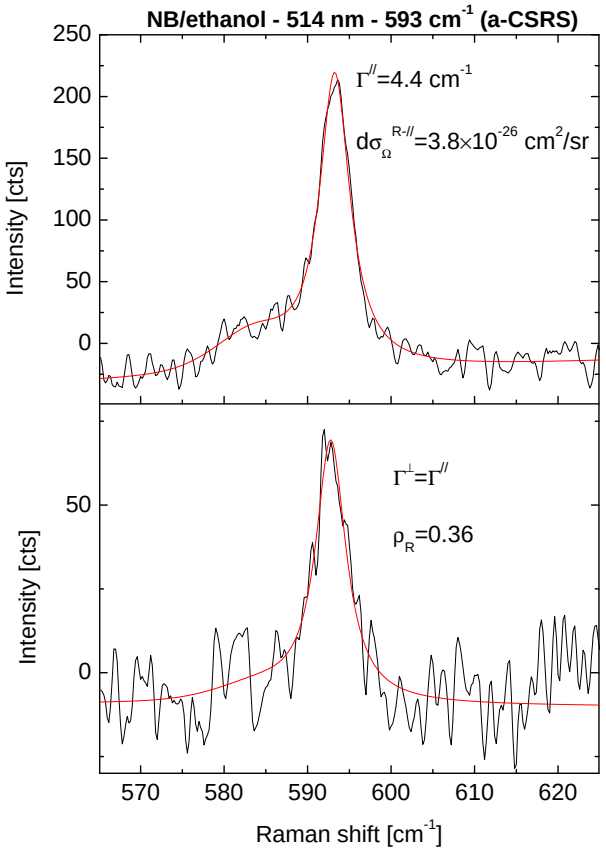

FIG. S16: CSRS measurement of the $593\,\mathrm{cm}^{-1}$ mode of NB in ethanol ($c = 5.1\,\mu$M) at 514 nm using 50 shifts of $1\,\mathrm{cm}^{-1}$. We show the a-CSRS spectra for parallel ($\|$) and perpendicular ($\perp$) polarizations, along with double Lorentzian fits (to account for the small peak on the low energy side of the main peak). We have here imposed $\Gamma^{\perp} = \Gamma^{\|}$ in the fit for $\perp$. The cross-sections are inferred by using the fluorescence background (not shown and dominated by extrinsic fluorescence here) as a reference as explained in the main text and in Eq. S7. We here have $R^{\|} = 1.9 \times 10^{-2}$ and independently measured $d\sigma^{F-\|}_{\Omega\bar{\nu}} = 2.8 \times 10^{-25}\,\mathrm{cm}^2/\mathrm{sr}/\mathrm{cm}^{-1}$ and $\rho^F = 0.84$. Note that the same Raman cross-section is derived when using the $884\,\mathrm{cm}^{-1}$ peak of ethanol as reference.

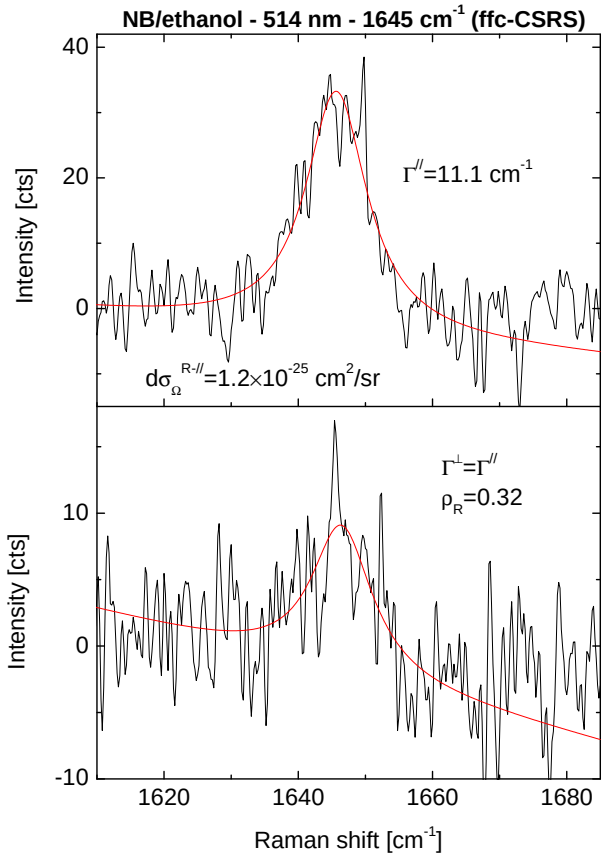

FIG. S17: CSRS measurement of the $1645\,\mathrm{cm}^{-1}$ mode of NB in ethanol ($c = 5.1\,\mu$M) at 514 nm using 40 shifts of $2\,\mathrm{cm}^{-1}$. We show the ffc-CSRS (with 2 iterations) spectra for parallel ($\|$) and perpendicular ($\perp$) polarizations, along with Lorentzian fits. We have here imposed $\Gamma^{\perp} = \Gamma^{\|}$ in the fit for $\perp$. The cross-sections are inferred by using the fluorescence background (not shown and dominated by extrinsic fluorescence here) as a reference as explained in the main text and in Eq. S7. We here have $R^{\|} = 1.3 \times 10^{-3}$ and independently measured $d\sigma^{F-\|}_{\Omega\bar{\nu}} = 5.3 \times 10^{-24}\,\mathrm{cm}^2/\mathrm{sr}/\mathrm{cm}^{-1}$ and $\rho^F = 0.88$.

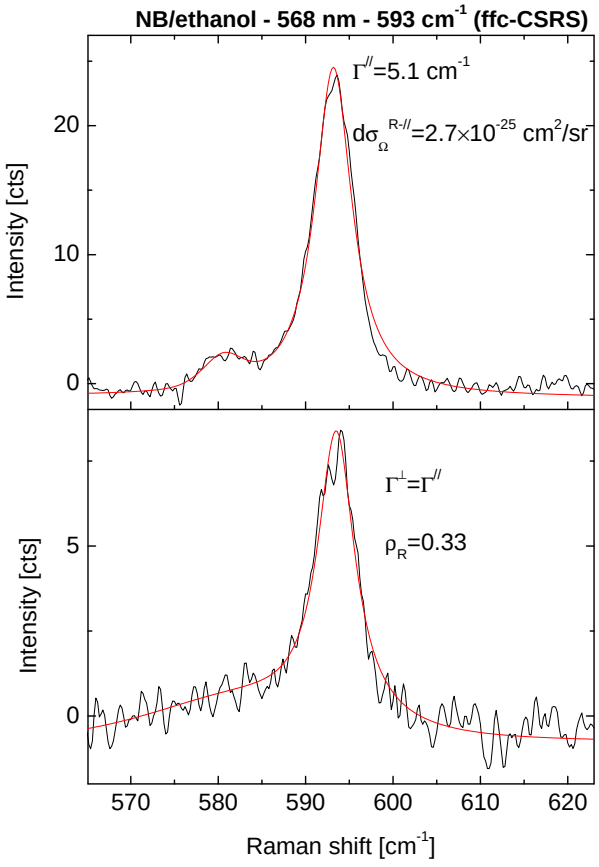

FIG. S18: CSRS measurement of the $593\,\mathrm{cm}^{-1}$ mode of NB in ethanol ($c = 5.1\,\mu$M) at 568 nm using 50 shifts of $1\,\mathrm{cm}^{-1}$. We show the ffc-CSRS spectra for parallel ($\parallel$) and perpendicular ($\perp$) polarizations, along with double Lorentzian fits (to account for the small peak on the low energy side of the main peak). We have here imposed $\Gamma^{\perp} = \Gamma^{\parallel}$ in the fit for $\perp$. The cross-sections are inferred by using the fluorescence background (not shown and dominated by extrinsic fluorescence here) as a reference as explained in the main text and in Eq. S7. We here have $R^{\parallel} = 3.2 \times 10^{-3}$ and independently measured $d\sigma^{F-\parallel}_{\Omega\tilde{\nu}} = 1.05 \times 10^{-23}\,\mathrm{cm}^2/\mathrm{sr}/\mathrm{cm}^{-1}$ and $\rho^F = 0.84$. Note that the same Raman cross-section is derived when using the $884\,\mathrm{cm}^{-1}$ peak of ethanol as reference.

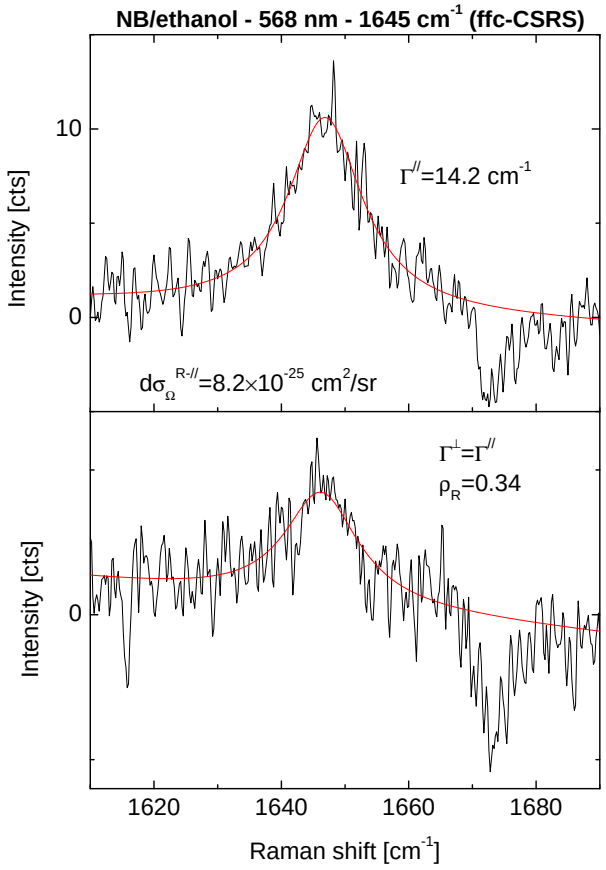

FIG. S19: CSRS measurement of the $1645\,\mathrm{cm}^{-1}$ mode of NB in ethanol ($c = 5.1\,\mu$M) at 568 nm using 40 shifts of $2\,\mathrm{cm}^{-1}$. We show the ffc-CSRS (with 2 iterations) spectra for parallel ($\parallel$) and perpendicular ($\perp$) polarizations, along with Lorentzian fits. Note the water absorption line on the high energy side of the peak. We have here imposed $\Gamma^{\perp} = \Gamma^{\parallel}$ in the fit for $\perp$. The cross-sections are inferred by using the fluorescence background (not shown) as a reference as explained in the main text and in Eq. S7. We here have $R^{\parallel} = 4.3 \times 10^{-4}$ and independently measured $d\sigma^{F-\parallel}_{\Omega\tilde{\nu}} = 8.7 \times 10^{-23}\,\mathrm{cm}^2/\mathrm{sr}/\mathrm{cm}^{-1}$ and $\rho^F = 0.9$.

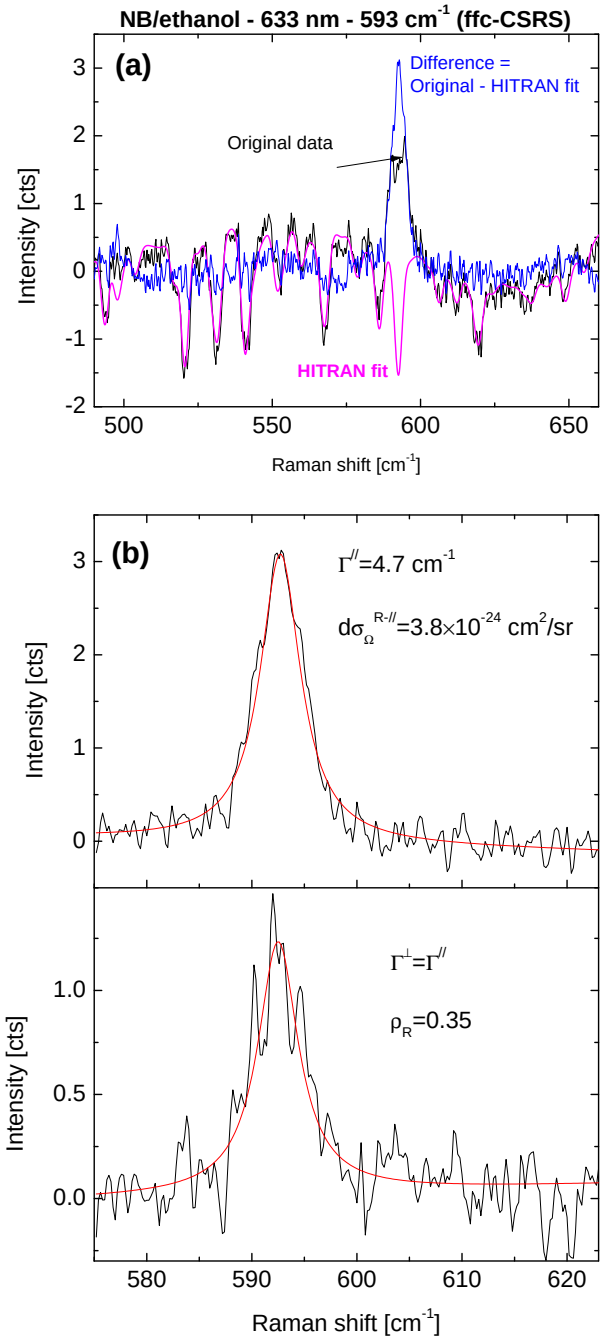

FIG. S20: CSRS measurement of the 593 cm^{-1} mode of NB in ethanol ($c \approx 3\,\mu$M) at 633 nm using 50 shifts of 1 cm^{-1} with 132 s ($\parallel$) and 148 s ($\perp$) integration per shift. In the raw spectra shown in (a), although the Raman peak is visible, water vapour absorption lines are also clearly visible and may affect the spectrum. We therefore illustrate how these can be, at least partially removed, by fitting the results with absorption predictions computed from the HITRAN database [7], as shown also in (a). The resulting spectra in (b) (shown with Lorentzian fits) are less affected by the absorption lines and are quantitatively different from the raw spectra, notably because of the absorption band at 593 cm^{-1}, right in the middle of the Raman peak. We have here imposed $\Gamma^{\perp} = \Gamma^{\parallel}$ in the fit for $\perp$. The cross-sections are inferred by using the fluorescence background (not shown) as a reference as explained in the main text and in Eq. S7. We here have $R^{\parallel} = 3.1 \times 10^{-4}$ and independently measured $d\sigma^{F-\parallel}_{\Omega\bar{\nu}} = 1.65 \times 10^{-21}\,\mathrm{cm}^2/\mathrm{sr}/\mathrm{cm}^{-1}$ and $\rho^F = 0.88$. Note that the obtained Raman cross-section is in agreement with the one obtained in Ref. 1 using PD-RRS.

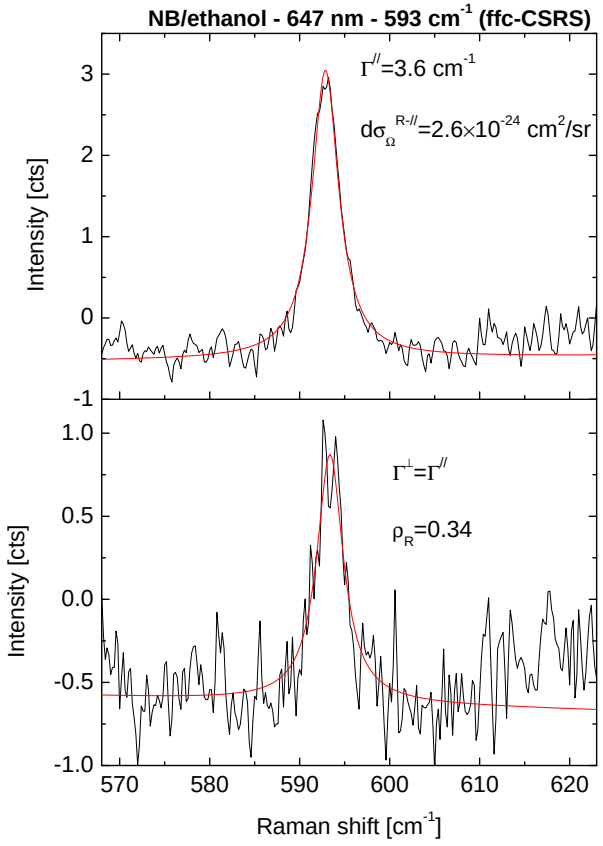

FIG. S21: CSRS measurement of the 593 cm^{-1} mode of NB in ethanol ($c \approx 3\,\mu$M) at 647 nm using 50 shifts of 1 cm^{-1} with 75 s ($\parallel$) and 46 s ($\perp$) integration per shift. We show the ffc-CSRS (with 2 iterations) spectra for parallel ($\parallel$) and perpendicular ($\perp$) polarizations, along with Lorentzian fits. We believe the remarkably narrow linewidth observed is real and is a result of particularly good alignment conditions for this measurement. The cross-sections are inferred by using the fluorescence background (not shown) as a reference as explained in the main text and in Eq. S7. We here have $R^{\parallel} = 3.8 \times 10^{-4}$ and independently measured $d\sigma^{F-\parallel}_{\Omega\bar{\nu}} = 1.2 \times 10^{-22}\,\mathrm{cm}^2/\mathrm{sr}/\mathrm{cm}^{-1}$ and $\rho^F = 0.87$.

[1] E. C. Le Ru, L. C. Schroeter, and P. G. Etchegoin, Anal. Chem. **84**, 5074 (2012).
[2] M. K. Lawless and R. A. Mathies, J. Chem. Phys. **96**, 8037 (1992).
[3] S. Shim, C. M. Stuart, and R. A. Mathies, ChemPhysChem **9**, 697 (2008).
[4] E. C. Le Ru and P. G. Etchegoin, *Principles of Surface Enhanced Raman Spectroscopy and Related Plasmonic Effects* (Elsevier, Amsterdam, 2009).
[5] R. L. McCreery, *Raman Spectroscopy for Chemical Analysis* (John Wiley & Sons, Inc., 2005).
[6] E. C. Le Ru, E. Blackie, M. Meyer, and P. G. Etchegoin, J. Phys. Chem. C **111**, 13794 (2007).
[7] L. Rothman, I. Gordon, A. Barbe, D. Benner, P. Bernath, M. Birk, V. Boudon, L. Brown, A. Campargue, J.-P. Champion, et al., J. Quant. Spectrosc. Rad. Transf. **110**, 533 (2009).
[8] B. Auguié, A. Reigue, E. C. Le Ru, and P. G. Etchegoin, Anal. Chem. **84**, 7938 (2012).